Universitetet i Stavanger

FACULTY OF SCIENCE AND TECHNOLOGY

MASTER'S THESIS

Study programme/specialisation: Petroleum Engineering / Well Engineering	Spring semester, 2018 Open
Author: Milton Eduardo Angulo Cruz	…… (signature of author)
Programme coordinator: Supervisor(s): Rune W. Time Herimonja A. Rabenjafimanantsoa	
Title of master's thesis: Surface Tension Measurement by Maximum Bubble Pressure Method	
Credits: 30	
Keywords: Surface tension Noise analysis Image processing	Number of pages: 74 Stavanger, 15.06.18

Surface Tension Measurement by Maximum Bubble Pressure Method

Contents

Summary

The principal objective of the present work is to measure the surface tension of liquids by the use of a method that it is not commonly found in books but it is based on very basic principles of Fluid Mechanics. This thesis is purely experimental. The measurement of the surface tension by The Maximum Bubble Pressure Method can be implemented with basic laboratory equipment on its simplest configuration but if a detailed analysis is desired can also be implemented with more advanced equipment to see what is involved inside the experiment, this also implies a higher level of complexity on data processing and understanding of the results.

In order to test the method, it was decided to use fluids that can be easily found in the laboratory and within the largest possible range of values of surface tension. These fluids are pure water, solutions of ethanol with a concentration of 10% and 30% in weight, n-Octane and n-Hexane.

The principle of the method is to inject air through a capillary tube with known radius that is submerged in a fluid at different depths, the maximum value of the injection pressure is recorded and the surface tension can be calculated. Based on this, some layouts were tested not only to measure these values but also to see how the bubble is formed over time with a slow-motion camera and how the pressure and temperature behave along the time with sensors attached to a computer. Several configurations and equipment were tested until obtaining the final distribution that meets the requirements.

Once the data was acquired, it was necessary to analyze the quality of it. Since the pressure and temperature signals were recorded by computer, some noise associated with the data acquisition was observed. For this reason, filtering techniques such as Low Pass Filter, Moving Average Filter and Fast Fourier Transform were implemented in a successful attempt to improve the reliability of the data. From the images captured by the slow motion camera it is possible not only to measure the dimensions of the bubble but to see how the interface between air and liquid behaves along the time.

The results obtained are shown in Table 1, it can be observed that the associated error to the calculations is no larger than 5.73%. Finally, the possible reasons of these errors are briefly discussed.

Table 1: Sumary of results

Fluid	Reference Value, mN/m	Measured value, mN/m	% Error
Water	71.87	70.68	1.66%
Ethanol 30%w	33.04	33.86	2.48%
Ethanol 10%w	48.21	47.90	0.64%
n-Hexane	17.81	17.29	2.92%
n-Octane	20.93	19.73	5.73%

Acknowledgment

The present work was written as part of the completion of a two-year program to obtain the Degree of MSc in Petroleum Engineering with specialization in Well Engineering. Since the university has state of the art equipment in addition to qualified personnel, I chose to write my thesis with the University of the Stavanger because I wanted to perform an experimental work. During the previous semesters I met many teachers, I contacted some of them to raise my idea of an experimental thesis and finally decided to do it with Prof. Rune Time. He offered me some topics and I picked one related to Fluid Mechanics.

I would like to thank the following people:

Senior Engineer Herimonja A. Rabenjafimanantsoa, for his help in the assembly of the equipment and his support in the writing part, pushing me every single day to fulfill this work.

Professor Rune W. Time, for his willingness in sharing his scientific knowledge and his guidance to reach the initial objectives.

To my friend MSc. Juan Carlos Jimenez, for his patience in explain me how to perform an adequate signal processing despite of being ten thousand kilometers far from Stavanger.

To Diego who has been like a brother and to all my friends that I made in the university during these last two years, for the support they offered me to finish this stage in my life.

I dedicate this work to my beloved family, without them all my achievements mean nothing.

Nomenclature

Abbreviations

MBPM	Maximum Bubble Pressure Method
FFT	Fast Fourier Transform
LPF	Low Pass Filter
MAF	Moving Average Filter
FPS	Frames per second
SLN	Solution
Z_c	Height of the bubble
h_A	Capillary tube depth
r	Bubble radius
Wc	Cutoff frequency (LPF)
n	Samples to be averaged (MAF)
Ø	Diameter
L	Length
ΔP_{MAX}	Maximum Delta Pressure
σ	Surface tension
β	Correction factor for surface tension calculation
ρ_A	Fluid density
g	Gravity acceleration

List of figures

Chapter 1

1. Introduction

The determination of some physical properties like density, viscosity, compressibility, elasticity, vapor pressure and surface tension are key factors on fields related to research and industry. When we talk about small-scale processes, it can be affirmed that the surface tension plays an important role since these forces are larger than the gravitational forces. This can be seen in many fields of biology, environmental science and technology.

Several examples can be given: all the small living creatures live in an environment mainly dominated by surface tension, some animals and plants have developed natural strategies for water-repellency, dynamics of magma chambers and volcanoes, the dynamics of raindrops and their role in the biosphere, the design of ways to coat the insects and leave the plant unharmed in the fight against plagues, application of cavitation in medicine to treat tumors and kidney stones, coating technology to repel dust and water, among others. [1]

Inside the Petroleum Industry, there are many fields where the surface tension plays an important role. Inside the pore space on the reservoir rocks, the distribution and the flow of the fluids is highly influenced by the wettability of the rock, property directly related to the surface tension. In addition, during the well drilling process and workover operations it is important to use an appropriate fluid. The use of surfactants that modifies the surface tension is common. By understanding the way these fluids interact with the reservoir rock in the zone close to the wellbore is a key factor for the success of an operation, otherwise the pore space can be clogged and left the well with limited or no productivity. On the opposite way, a proper comprehension of the fluid properties at downhole conditions and the way they interact with other fluids will result in a successful job.

As a preparation for this thesis to obtain a background knowledge and improve the understanding of all the variables involved in this experiment, there were read some articles about experiments for the determination of the surface tension, some of them with very basic theory and knowledge about what it is involved in the process of the measurement using this method, and other recent articles with more advanced techniques. Much has been said in these documents and publications by the use of basic laboratory equipment for acquiring the data that somehow limited the capacity of the analysis. By the use most recent technology in data acquisition, it can be understood in a better way all the variables involved in the process

of determining the surface tension. This motivates to analyze these aspects by the use of state of the art equipment: temperature sensors and pressure transducers with a high resolution and fast sampling rates, slow-motion cameras, digital image processing, among others. Since the formation and expansion of a bubble takes only a few milliseconds, the use of the techniques previously mentioned will help not only to perform the measurement of the surface tension but to analyze and describe the phenomena and peculiarities around this experiment. To perform an adequate processing of the measurements obtained from the experiment it is recommended the use of MATLAB because a code can be developed to perform filtering of the signals and noise analysis from the pressure and temperature measurements, and identify the movement of the interface along the time with a proper image analysis.

The present thesis work is organized as follows:

Chapter 2 presents basic definitions about surface tension and some methods used to measure it with a detailed description about the Maximum Bubble Pressure Method. Additionally, the principles of signal processing and definition of Newtonian and non-Newtonian fluids are presented.

Chapter 3 describes the criteria for the selection of the parts to perform the experiments, the way they were put together to record data and how the signals will be treated to calculate the surface tension.

Chapter 4 includes the processing of all the data to validate it and the calculations of surface tension for different fluids. Additionally, the possible causes for errors are analyzed.

Chapter 5 shows the conclusions obtained from the experiments.

Appendix A includes Matlab scripts used to process the data.

Appendix B shows some illustrations from the experiment.

Chapter 2

2. Theory

In this chapter, basic definitions about surface tension are cited. Additionally, a brief summary about several methods to determine surface tension with special focus on the Maximum Bubble Pressure Method are explained. Since the data treatment is mandatory in order to have good results, techniques of signal processing are discussed. Finally, the definitions of Newtonian and non-Newtonian are also included.

2.1 Surface tension

The molecules inside a liquid are attracted to each other. At the surface, these are subject to strong attractive forces exerted by other molecules in their vicinity. The resultant of these attractive forces acts in a plane which is tangent to the surface at a particular point. The magnitude of this resultant force acting perpendicular to a line of unit length in the surface is known as surface tension, σ.

A more physically appealing definition of surface tension exists. Considering that a certain amount of energy is required to reach below the free surface of a liquid and pull molecules upward to the surface to form a new area. The energy required per unit area formed is defined as surface tension [2].

Surface tension has the units of force/length or equivalent energy/area: J/m^2 = N/m. The common unit used to report values is milinewton per meter mN/m. It is normally discriminated between *interfacial tension* between two phases, and the *surface tension* on the surface of a medium against vacuum. Often surface tension is used for the liquid phase and its saturated vapor in air [3].

Considering the concept of surface tension in terms of energy per unit area, in the absence of gravitational or other fields, a soap bubble is spherical, as this is the shape of minimum surface area for an enclosed volume. The "virtual work method" which states that *at equilibrium, a small work from the bubble must equal the change in surface energy* [3] will be used to derive some equations. A soap bubble of radius *r* has a total surface free energy of $4 \cdot \pi \cdot r^2 \cdot \sigma$ and, if the radius is decreased by *dr*, then the change in surface free energy would be

$8 \cdot \pi \cdot r \cdot \sigma \cdot dr$. Since shrinking decreases the surface energy, the tendency to do so must be balanced by a pressure difference across the film ΔP such that the work against this pressure difference $\Delta P \cdot 4 \cdot \pi \cdot r^2 \cdot dr$ is just equal to the decrease in surface free energy. Thus:

$$\Delta P \cdot 4 \cdot \pi \cdot r^2 \cdot dr = 8 \cdot \pi \cdot r \cdot \sigma \cdot dr$$

or

$$\Delta P = \frac{2 * \sigma}{r} \tag{1}$$

According to the previous equation, it can be said that the smaller the bubble, the greater the pressure of the air inside relative to that outside [4].

In case of a curved surface that is not spherical but ellipsoidal, Young and Laplace developed an equation that takes this into consideration, based on the two principal radii [4]:

$$\Delta \mathrm{P} = \sigma \left(\frac{1}{\mathrm{R}_1} + \frac{1}{\mathrm{R}_2} \right) \tag{2}$$

2.2 Dependence of interfacial tension on pressure and temperature

Interfacial tension is more sensitive to temperature than to pressure. A common correlation to relate interfacial tension between two reduced temperatures T_{r1} and T_{r2} is given by [3]:

$$\frac{\sigma_1}{\sigma_2} = \left[\frac{1 - \mathrm{T_{r1}}}{1 - \mathrm{T_{r2}}} \right]^{1.2} \qquad (\mathrm{T} < \mathrm{T_c}) \tag{3}$$

where the reduced temperature is given by $T_r = T / T_c$ and T_c is the critical temperature. Note that for liquid the reduced temperature is less than 1. The interfacial tension decreases with increasing temperature of the liquid. Figure 1 shows the temperature dependence of the vapor-liquid surface tension for some fluids.

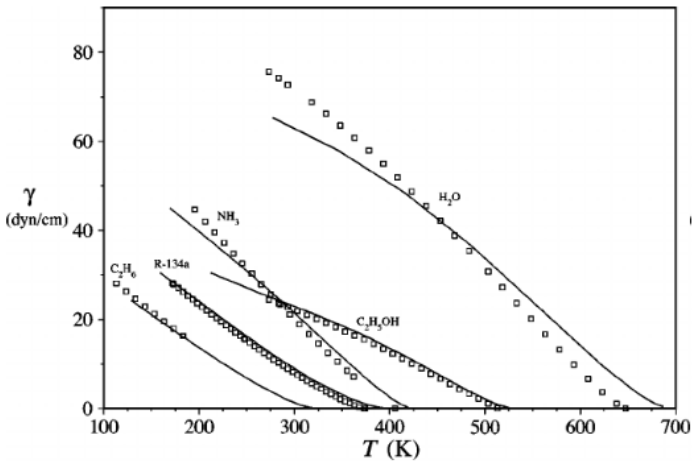

Figure 1: Temperature dependence of the vapor-liquid surface tension for some fluids [5].

The interfacial tension varies with pressure by two mechanisms, that both contribute to reducing σ when pressure increases:

1. Pressure increase increases the amount of dissolved gas in liquid.

2. The gas density increases with increasing pressure thus in total the density difference between gas and liquid decreases [3].

2.3 Surface tension measurement

Along the years, there has been a variety of techniques used to measure interfacial tensions between immiscible fluid phases. These techniques can also be applied to measure the surface tension. Some of them can be used to measure dynamic interfacial tension in fluids that their composition is constantly refreshed and doesn't reach the equilibrium. The scope of the present work is focused in analyzing fluids that have a stable value of surface tension.

The most common techniques can be classified in different groups as shown on Figure 2. A brief description of these techniques is mentioned below according to the investigation presented by Michigan Technology University [6].

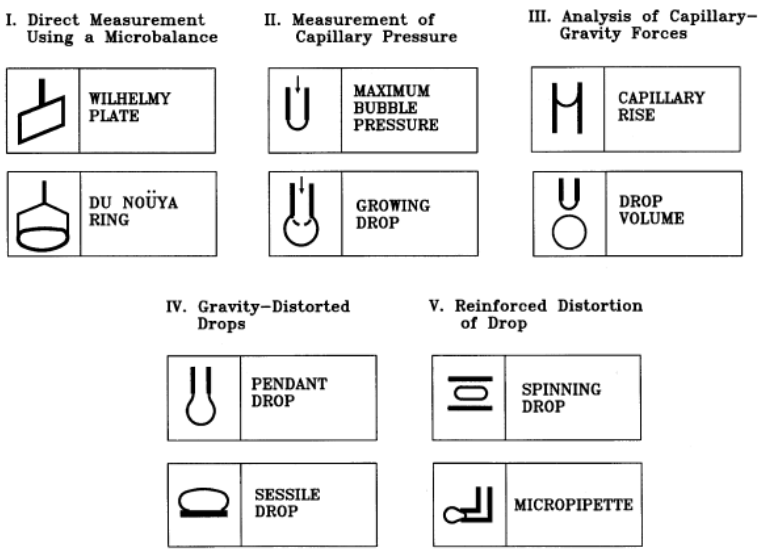

Figure 2: Classification of techniques for interfacial tension measurements [6].

2.3.1 Direct Measurement Using a Microbalance

Interfacial tension at fluid-fluid interfaces is a reflection of the excess energy associated with unsaturated intermolecular interactions at the interface [6]. This excess energy tends to drive interfaces to adopt geometries that minimize the interfacial area, and this tendency can be interpreted as a physical force per unit length (i.e., a tension) applied in the plane of the interface. The excess energy per unit area (E/A) is numerically equal to this force per unit length (F/L), which is numerically equal to the interfacial tension.

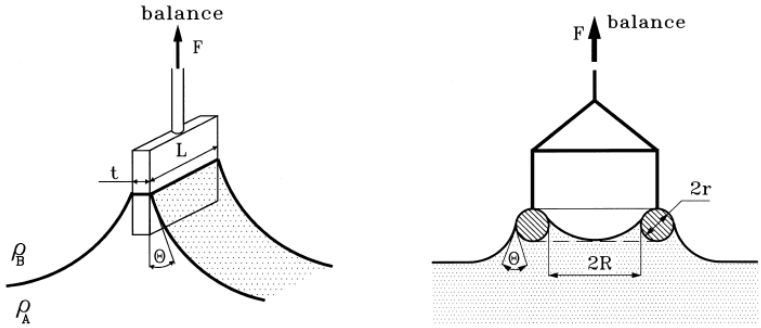

Figure 3: Schematic of Wilhelmy plate method (left) and Du Noüy ring method (right) [6].

Whihelmy plate technique: A vertical thin plate is put in a fixed position relative to the horizontal surface of the liquid. A force (F) vertically acting on the plate by the liquid meniscus is measured by using a microbalance, as shown on the Figure 3 left. The force

applied to the plate is equal to the weight of the liquid meniscus uplifted over the horizontal surface. By measuring this force the interfacial tension can be calculated.

Du Noüy ring method: In this method, the interfacial tension relates to the force required to pull a wire ring off the interface. To calculate an accurate value of surface tension it is necessary to know not only the force but also the perimeter of the ring and the thickness of the wire to determine correction factors. If all of the necessary experimental precautions are observed, this method can guarantee higher accuracy than any other detachment method. An illustration of this method is shown on the Figure 3 right.

2.3.2 Measurement of Capillary Pressure

Interfacial tension is defined as the work required to create a unit area of interface at a constant temperature, pressure, and chemical potential. Because it is always positive for interfaces between immiscible phases, interfacial tension always tends to decrease the area of interface. This tendency gives rise to a pressure difference between fluids on either side of a curved interface, with the higher pressure on the concave side of the interface. This pressure difference results in phenomena such as a capillary rise, bubble and drop formation, among others, that can be measured in a number of ways and then be used to calculate if the radius of curvature is known [6].

Maximum bubble pressure: This method is based on measuring the maximum pressure to force a gas bubble out of a capillary into a liquid. The measured pressure is the sum of capillary pressure caused by the interfacial tension and the hydrostatic pressure caused by the liquid column above the orifice of the capillary; with this value the surface tension can be calculated. This method is discussed in detail in the point 2.4 which is the main focus of this thesis.

Growing drop method: To use this method is necessary to measure the pressure inside a bubble precisely and continuously as it forms and detaches from the end of a capillary. This ability to simultaneously monitor both pressure and geometry (size and shape) of bubbles or drops as they form allows dynamic interfacial tensions to be evaluated over a range of growth rates by the use of a micropump to carefully control the growth rate of the drop or bubble. When this method is applied to systems in equilibrium, the surface tension can be obtained.

2.3.3 Balance between Capillary and Gravity Forces

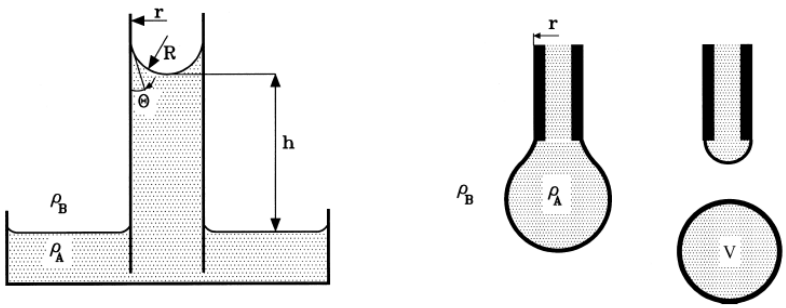

Figure 4: Schematic of Capillary rise method (left) and drop volume method (right) [6].

Methods based on analysis of capillary effects, other than the shape of a drop or meniscus, such as capillary rise and drop volume or weight, are among the oldest surface tension measurement methods in use [6].

Capillary rise method: The basis for this method is to measure the contact angle and the height of the meniscus in a round glass tube of a known inner radius, as can be seen on the Figure 4 left. This technique can be very accurate to measure surface tension but some problems related to fabrication of a uniform bare capillary tube and precise determination of the inside diameter may rise. This method is not recommended to measure the interfacial tension between two liquids.

Drop volume or weight: The weight or volume of a drop falling from a capillary with a known radius is measured (see Figure 4 right). This weight is correlated directly to the value of interfacial tension. To perform accurate calculations there is the need to use corrections factors for volume and it is recommended to collect many drops in order to have a good estimation in the value of weight or volume. The measurements of interfacial tension with this technique are very simple but are very sensitive to external factors such as vibrations and multicomponent solutions when adsorption occurs.

2.3.4 Gravity-Distorted Drops

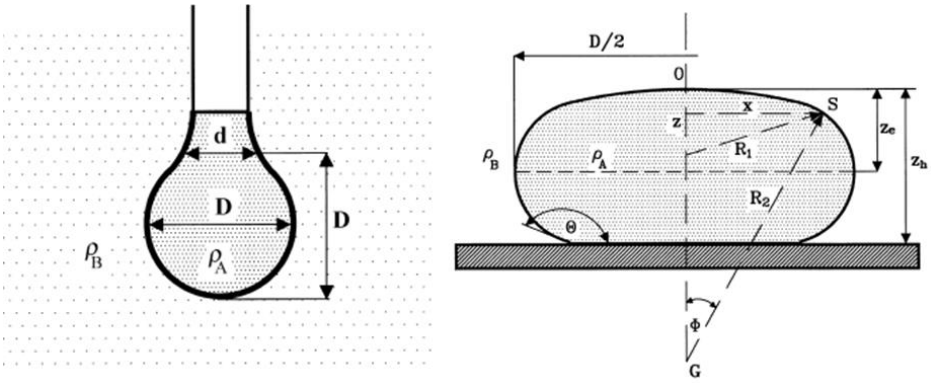

Figure 5: Schematics for pendant drop method (left) and sessile drop method (right) [6].

Interfacial tension causes interfaces to behave as elastic membranes that always tend to compress the liquid. In the absence of other forces (e.g., in zero gravity), the liquid surface has a natural tendency to form spherical shapes to minimize the interfacial area per unit volume of liquid and thus minimize the excess energy of the interface. The shape of an interface in a gravitational field depends on the competition between the capillary and gravitational forces. The techniques of curved interface shape analysis do not require advanced instrumentation. The experimental setup requires a camera with a low-magnification lens to record the shape of the drop. The interfacial tension can be easily calculated from the dimensions of the pendant drop (Figure 5 left), sessile drop (Figure 5 right), or liquid meniscus taken from the photographic picture and by using numerical solutions [6].

Pendant drop method: From the image processing and according to Figure 5 (left), the parameters of D and d are measured. With the values of the fluid densities, the interfacial tension can be determined. As all the other methods, cleanliness is a must in order to get good quality and reproducible results.

Sessile drop method: This method is based on the analysis of the profile of the drop sitting on a solid substrate, as shown in Figure 5 (right). On a simple approach, the principal parameter to be measured is the height from the top of the drop to its equator. To determine the surface tension from a practical point of view it is difficult to find the exact location of the equator and sometimes locating the top of the drop is experimentally difficult.

2.3.5 Reinforced Distortion of Drop.

These techniques to measure the interfacial tension are based on the distortion on the shape of fluid drops by centrifugal forces and can be used to measure ultralow interfacial tensions. These low values can be found in fluids used to perform enhanced recovery in the petroleum industry, for example, where the values can be as low as 1 mN/m. It is difficult to perform surface tension measurement in these fluids with the methods mentioned above. Therefore, there is a need to use alternative methods [6].

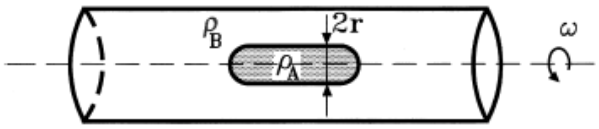

Figure 6: Schematic of the rotating drop method [6].

Spinning drop: This technique relies on the fact that gravitational acceleration has little effect on the shape of a fluid drop suspended in a liquid, when drop and the liquid are contained in a horizontal tube spun about its longitudinal axis as is shown on the Figure 6. At low rotational velocities, the fluid drop will take on an ellipsoidal shape, but when this velocity is sufficiently large, it will become cylindrical. Under this last condition, the radius of the cylindrical drop is determined by the interfacial tension, the density difference between the drop and the surrounding fluid, and the rotational velocity of the drop. As the result, the interfacial tension can be calculated. This has been successful in the measurement of surface tension values as low as 10^{-6} mN/m.

2.3.6 Microtensiometry

Microtensiometry is the study of interfaces on very small particles and in finely dispersed systems. In fields such as biology, pharmaceutical processing and nanotechnology, the common techniques of surface tension measurement can’t be applied. The study of interfaces on the nanometer scale may exhibit properties that are very different from their macroscopic counterparts [6].

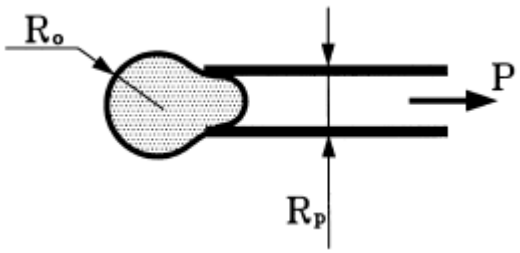

Figure 7: Illustration of the micropipette technique [6].

Micropipette Technique: This technique was developed for the direct measurement of interfacial tensions of micrometer-sized droplets. In this technique, the droplet is first captured at the tip of the glass micropipette and then sucked into the pipette as shown in the Figure 7. The interfacial tension is calculated from the minimum pressure at which the droplet extends a hemispherical protrusion into the pipette by using the Laplace Equation. There is also another variant of this experiment by the use of two pipettes to avoid the limitation of the large pressure difference required to draw the droplet into the pipette.

2.4 Maximum bubble pressure method

The procedure to perform this method is to slowly blow bubbles of gas by the use of a small tube that is submerged in a liquid and record the required pressure, as can be seen on the Figure 8. The bubble formed on capillary tip continually becomes bigger in surface and its radius is decreasing (Figure 8, A). When the pressure reaches a maximum level, the bubble has its minimum radius equal to the radius of the tube, forming and hemisphere (Figure 8, B). After this point, the bubble quickly expands and tears away from the tip of the capillary to start a new cycle (Figure 8, C) [7].

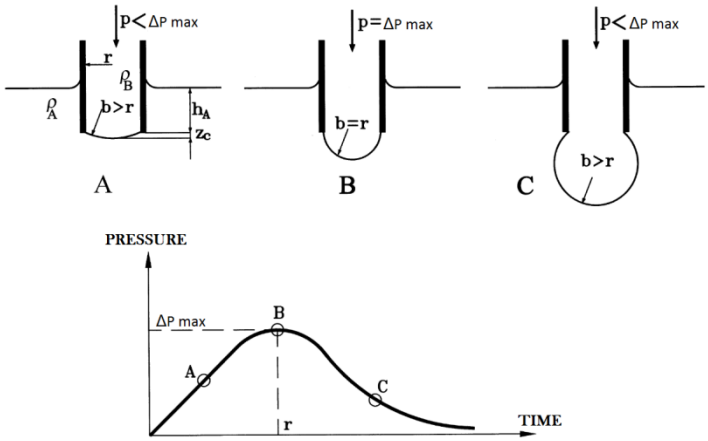

Figure 8: Maximum bubble pressure method [6].

Starting from the equation (1) under chapter 2 and having the values of the maximum pressure recorded, the capillary dimensions, the fluid density and the depth of immersion, it is possible to calculate the surface tension in an ideal case with the use of the next equation:

$$\sigma = \frac{r}{2}(\Delta P_{MAX} - h_A \cdot \rho_A \cdot g) \quad (4)$$

According to real cases, the values of surface tension estimated with the above equation won't be accurate because of the effect of gravity, bubble adhesion to the capillary, particles of moisture carried by the air and turbulence generated by the growth of the bubble itself, among others [8]. As described above, in the MBPM there is a tendency for the bubble to be deformed causing erroneous determination of the surface tension values. Therefore new method to perform calculations is needed.

2.4.1 Sugden approach

The parameters $(\Delta P_{max} - \rho_A \cdot g \cdot h_A)$ in equation (2) correspond to the value of the capillary pressure and can be expressed as the height *(h)* of the column of an imaginary liquid of density $(\Delta\rho = \rho_A - \rho_B)$:

$$h = \frac{\Delta P_{MAX} - \rho_A \cdot g \cdot h_A}{\Delta\rho \cdot g} \quad (5)$$

It can be related *h* with the Laplace capillary constant $a^2 = 2 \cdot \sigma/(\Delta\rho \cdot g)$ and the bubble meniscus:

$$\frac{r}{X} = \frac{r}{b} + \left(\frac{r}{a}\right)\left(\frac{Z_C}{b}\right)\left(\frac{\alpha}{2}\right)^{1/2} \quad (6)$$

where $X = a^2/h$, $\alpha = 2b^2/a^2$, Z_c is the height of the bubble, and *b* is the curvature radius at the apex (lowest point of the bubble). The minimum values of *r/X* as dependent of a given value of *r/a* where tabulated, within the range $0 < r/a \leq 1.5$. Using this table, the surface tension can be calculated by following an iteration procedure [6]. This procedure is limited for capillary tubes with small radius and shallow immersion depths.

2.4.2 Young-Laplace approach and correction factor

Another approach is by using the Young-Laplace equation (eq. (2)) assuming that $R_1 = R_2$ and performing an experimental correction. It is achieved through a calibration that results

from maximum bubble pressure measurements as function of the capillary depth. Taking into account the existing procedures for surface tension measurement, the obtained calibration allows surface tension measurements with capillaries of any diameter and any immersion capillary depth.

Starting from equation (4) and inserting a correction factor β to account for the bubble's lack of spheroidicity, the next equation can be obtained [8]:

$$\sigma = \frac{r}{2}(\Delta P_{MAX} - \beta \cdot h_A \cdot \rho_A \cdot g)$$

Rearranging parameters

$$\Delta P_{MAX} = \frac{2 \cdot \sigma}{r} + \beta \cdot h_A \cdot \rho_A \cdot g \quad (7)$$

This equation states that the surface tension is constant and the ΔP_{MAX} will vary linearly with the depth considering a constant correction factor.

2.5 Signal Processing

In signal processing, a filter is a device or process that removes some unwanted components or features from a signal. Filtering is a class of signal processing; the defining feature of filters is the complete or partial suppression of some aspects from the signal. Most often, this means removing some frequencies and not others in order to suppress interfering signals and reduce background noise [9]. Figure 9 illustrates how the filter works.

Figure 9: Filtering principle.

In the current work three filters will be used to perform analysis of the signals:

- Fast Fourier Transformation.
- Low pass filtering.
- Moving average filtering.

2.5.1 Fast Fourier Transform.

The Fast Fourier Transform is a fundamental mathematical operation for some disciplines such as telecommunications or physics. Without it, there would not be modern telecommunications, not only the Internet or mobile telephony, but conventional telephony itself which could not have evolved from a local call to long-distance calls.

Basically the Fourier transform convert any mathematical function to another domain, called frequency domain. This makes easier to treat and analyze functions in an alternative way:

- The signal is transformed to the frequency domain that implies decomposing the signal in the different frequencies that compose it.
- Viewing the signal in this domain makes it possible to identify and separate the noise, which may have only some frequency components, and therefore can be filtered.
- The signal is returned again to the time domain, having a signal clean of noise [10].

This can be depicted on the next example:

Consider the function $y = \sin(4t) + 0.3\sin(12t)$. The responses in time domain and frequency domain are shown in Figure 10. In time domain it is not so obvious to discover the signals from upper graph, while in the frequency domain it can be seen clearly as a union of two sine signals with different frequencies and amplitudes [9] as shown in Figure 10 lower.

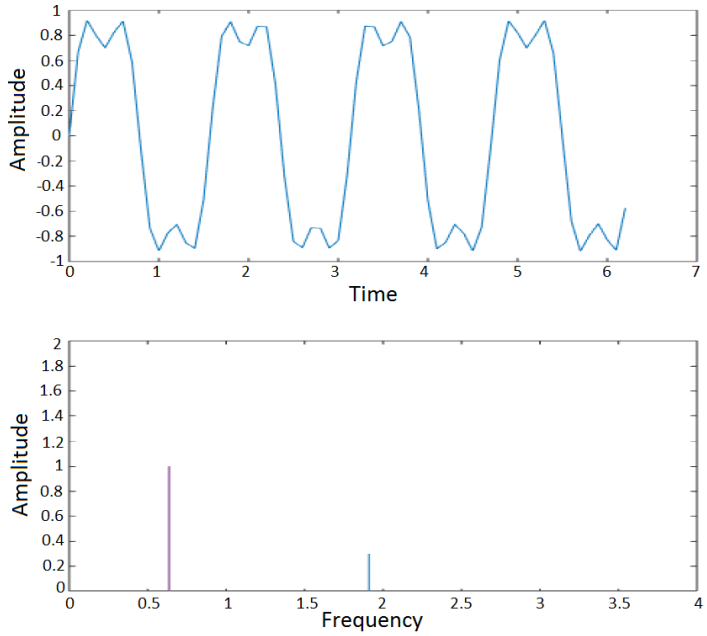

Figure 10: Function in time domain (upper) and frequency domain (lower) [9].

2.5.2 Low pass filter

A low-pass filter (LPF) is a filter that passes signals with a frequency lower than a certain cutoff frequency (*Wc*) and attenuates signals with frequencies higher than the cutoff frequency. The exact frequency response of the filter depends on the filter design.

There are two regions that are separated by the cutoff frequency: the passband and the stopband. The passband is the range of frequencies that is passed by the filter, and the stopband is the range of frequencies that is stopped by the filter. This can be seen in Figure 11.

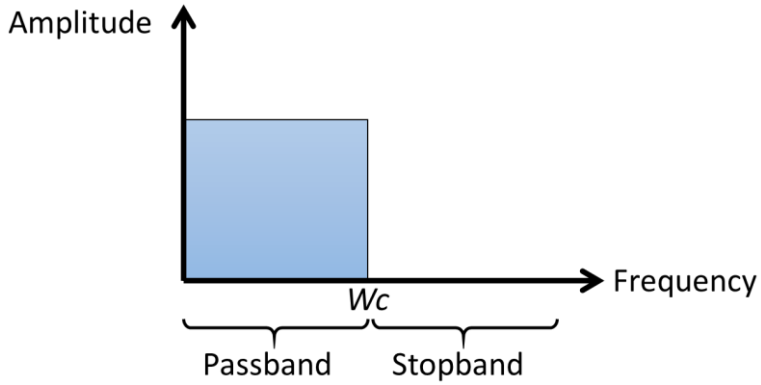

Figure 11: Low pass filter principle.

The LPF filtrates the high-frequency component out of the signal, and therefore this filter is useful for removing high frequency noise. Although the signal noise is reduced, the resulting signal is delayed compared to the original signal [9].

With a small value of *Wc*, the signal is smoothed but some valuable data can be lost in this process. On the other hand, a large value of *Wc* allows the entrance of more noise in the filtered data.

2.5.3 Moving average filter

The moving average filter (MAF) is a simple LPF commonly used for smoothing an array of sampled data/signal. This method takes *n* samples of input at a time, takes the average of those n-samples and produces a single output point. With the increase of *n*, the more noises with high frequencies will be stopped. In the same way as in the LPF case, a large value of *n* produces a smooth output but the delay effect becomes larger, additionally some data can be lost [9].

2.6 Fluids

2.6.1 Newtonian fluids

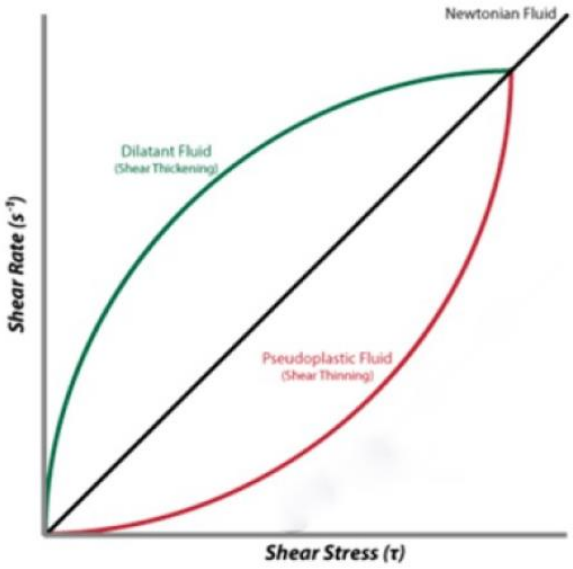

Figure 12: Comparison of Newtonian and Non-Newtonian fluids [11].

A Newtonian fluid is a fluid which exhibits a linear relation between the applied shear stress, τ and the shear rate γ. The relation is given by:

$$\tau = \mu\gamma$$

Where the proportionally constant μ is the viscosity of the fluid. A representation of this relation can be found as the black curve in Figure 12. In Newtonian fluids, the viscosity is only temperature and pressure dependent [12]. In this thesis, five fluids were analyzed; all of them are Newtonian fluids in order to simplify the calculations.

2.6.2 Non-Newtonian fluids

A non-Newtonian fluid is a fluid which exhibits a non-linear relation between the applied shear stress, τ and the shear rate γ. In non-Newtonian fluids, the viscosity, in addition to temperature and pressure, is shear stress and shear rate dependent [12].

There are mainly three types of non-Newtonian fluids. Figure 12 shows the comparison between these fluids relative to a Newtonian fluid.

- **Plastic.** Shear-thinning fluids, which means that the viscosity decreases as the shear rate increases.
- **Pseudoplastic.** Also shear-thinning fluids, but the transition between plastic and pseudoplastic can be hard to distinguish.
- **Dilatant.** Shear-thickening fluids, which means the viscosity increases as the shear rate increases [13].

In this thesis, none of the analyzed fluids is non-Newtonian fluid. Inside the experiment there are many things that are happening very fast, for example the formation of the bubbles. This will produce high shear in non-Newtonian fluids and these measurements will be affected by viscosity effects.

Chapter 3

3. Experimental Setup and Methods

This chapter discuss how were chosen all the elements to build the equipment to perform the experiment. Once this was done, the way the equipment was assembly and the configuration parameters are analyzed. Finally, the methods to process the data and the technique used to calculate the surface tension are shown.

3.1 Equipment selection criteria

In this part the necessary parts to build the layout of the experiment will be analyzed. Then, we will study the available options for each part and finally justify why each element was chosen.

3.1.1 Fluids

According to the theory in Chapter 2, this method to measure surface tension is applicable only to Newtonian fluids. With the purpose of having a range of different values of surface tension, five fluids were chosen. These are shown on the Table 2 with their respective reference at different temperatures. These fluids are easily obtained on any lab and don't represent a high risk to health when working with them adequately.

Table 2: Surface tension values

Fluid	Surface tension mN/m		
	20 ˚C	**25 ˚C**	**30 ˚C**
Water [14]	72.74	71.98	71.19
Ethanol 10%w [15]	48.14	47.53	46.88
Ethanol 30%w [15]	33.53	32.98	32.43
n-Octane [16]	21.61	21.14	20.20
n-Hexane[17]	18.47	17.90	17.26

3.1.2 Air source

To perform the experiments, air source is needed to create the bubbles inside the fluid to be analyzed. The air flow should be continuous over the time with enough pressure and a device to control the flow. Many options were analyzed and will be mentioned below:

Syringe: A common syringe was the first device tested as an air source for the experiment. The advantage is its low cost. The volume of air can be measured only by looking at the printed scale on the outside but since the plunger is controlled by hand, the flowrate was not constant and was discarded.

The use of a plunger controlled by a screw was also attempted. In every turn there was a controlled displacement of the volume evacuated by the piston. This option was also discarded because it had to be done manually and the automation of this mechanism would be possible but complex. Hence, the repeatability of experiments would be challenging. Moreover, the syringe has to be disconnected from the hoses to be filled again with air which is a time consuming operation and the seal can be damaged by doing this maneuver constantly.

Rubber bulb: A rubber bulb is a device that can be found in any laboratory and is widely used not only as a vacuum source for filling but also to control the flow of liquid by squeezing it. One of the main disadvantages with this device is that it's required to be detached from the experiment and to be filled again with air when a standard rubber bulb is used. By the use of a flip style pipette filler that is mainly a rubber bulb with a two valve system, there is no need to disconnect to allow the air to flow through. Despite the characteristics mentioned above, both options were discarded because they need to be manually squeezed which did not produce a constant flow of air.

Bottletop dispenser: This device is mainly used in laboratory to dispense a fixed amount of liquid. Externally has a glass piston attached to a scale (see Figure 13 left), internally has a pair of check valves that help to pump the fluid from inside the bottle to the outlet port (see Figure 13 right). The model available on the laboratory was a "Chempette® – Bench Dispenser" with a maximum volume of 10 ml per each piston trip [18]. Even though this device is intended to be used with liquids, it was tested with air and gave positive results. Once the glass piston is lifted it falls by its own weight because of the gravity and produces a constant flow of air. Additionally, this model of dispenser has its own fluid inlet and there is no need to disconnect any hose to refill the bottle.

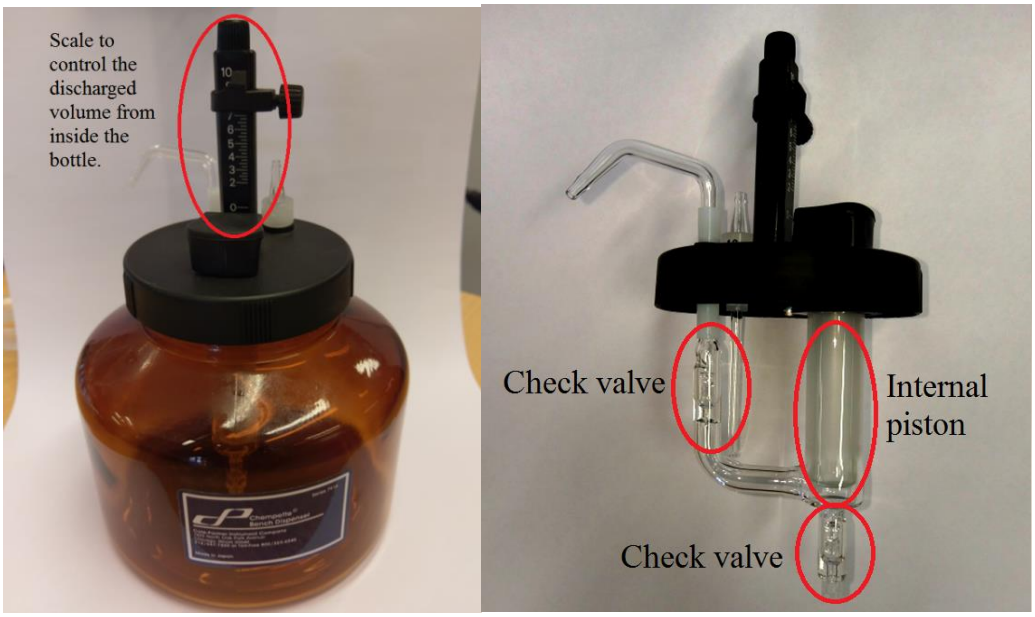

Figure 13: Bottletop dispenser (left) and its internal mechanism (right)

3.1.3 Container

The fluid to be analyzed needs to be inside a container to perform the experiment. Since a camera will be used visualize the bubble formation, it is mandatory to avoid any distortion on the visualization. Therefore, a low index of refraction is required. Another important feature that was taken into consideration is the resistance of the material when exposed to the analyzed fluid.

Glass beaker: This is cylindrical container with a flat bottom and it can be found in any laboratory with basic equipment. It is commonly made of glass or plastic. Even though the resistance to chemicals is good, this option was discarded because of its cylindrical shape that will interfere when taking pictures of the bubbles.

Glass cube: To avoid any distortion on the images to be recorded, a flat surface is desired. A cubic shape for the container would give satisfactory visual result. A glass cube was considered to be built due to its low index of refraction and resistance to chemicals. This option was finally discarded because the construction will take some time and there was another option of a plastic cube that was ready to be used.

Plastic cube: As mentioned above, a cubic shape as seen in Figure 14 was desired to allow a good high speed video recording. In the laboratory, a plastic cube was available which had an adequate dimension. The transparency of the walls was optimal without causing a blurry image. In order to make sure that the fluids to be analyzed won't react with the material of the

container jeopardizing the quality of the images, fluid samples were left for 24 hours and no reaction was observed. The dimensions of the cube are 75 mm x 75 mm x 96 mm (width, length and tall) with a wall thickness of 4.5 mm.

Figure 14: Plastic cube filled with water

3.1.4 High speed recording and visualization equipment

Part of this experiment is to perform an image processing when the bubbles are forming on the tip of the capillary. This phenomenon takes only a few milliseconds. The use of a camera with the capacity of taking enough images in a small period of time is then necessary.

Phone camera: The phone tested was a HTC 10 released on April 2016 that has a camera with the capacity to record a video with a vertical resolution of 720 pixel and an aspect ratio of 16:9 at a speed of 120 fps. It can focus objects at a minimum distance of 7 cm [19]. This option was discarded because the recording speed was not fast enough to the purposes of the experiment.

Slow-motion camera: A BASLER acA800-510uc camera as seen in Figure 15 that can record up to 511 fps [20] with a resolution up to 800 x 600 pixel (W x H) was tested and used. It was capable to focus objects up to 6 cm, it was connected to a computer using a USB 3.0 port and enough free space on the hard drive is necessary due to the large amount of pictures to be recorded. Under testing, it was found that the camera can’t record at 500 fps when it is at full resolution even though the illumination was good. This problem was fixed by reducing the resolution.

Light source: According to the US Department of Energy [21], incandescent bulbs release 90% of their energy as heat and compact fluorescent lamps release about 80% of their energy as heat. This is not desired since we are going to measure a parameter that depends on the temperature. For this reason, it was chosen a lamp with a gas discharge bulb technology: no filament – shockproof and unaffected by magnetic fields [22]. The model available at the laboratory is a LABINO AB, H135. Although this is a very efficient light source it generates a little amount of heat. Further analysis will be performed in the Chapter 4.

Figure 15: Slow-motion camera, BASLER acA800-510uc.

3.1.5 Pressure and temperature measurements

A mechanism to measure and record the pressure and temperature data as well as to visualize and perform the analysis of the data is important in this study. A common technique for pressure measurement would be with the use of a U tube filled with a fluid, one end connected to the air source and the other end open to the atmosphere. The difference on the liquid levels will give the value of the relative pressure [8]. This method was discarded. There is a need to perform measurements while the bubble is in formation which happens within a few milliseconds. This situation can only be achieved by the use of a transducer attached to the system to record the data. On the same way, the use of a standard thermometer would be the basic way to measure temperature. To record these data simultaneously the need of digital data acquisition equipment must be satisfied. Since the camera has the capacity of record 500 images in one second, it would be required a pressure sensor with similar or superior sampling rate. In the laboratory there is equipment capable to do this and will be described below.

PASCO Universal Interface as seen in Figure 16, is a data acquisition device. It is provided with digital and analog inputs, PASPORT sensor ports, a 15 W function generator, among other features [23]. It is designed specifically to be used in conjunction with PASCO Capstone software that allows the configuration of the sensors, display the data and analysis of them. There are a wide range of PASPORT sensors to measure physical variables. At the beginning the Absolute Pressure Temperature Sensor (PS-2146) was tested (see Figure 16, middle). This sensor has a sampling rate of 100 Hz which is not fast enough for the purposes of the experiment. The Dual Pressure Sensor (PS-2181) (see Figure 16, right) that allows a sampling rate up to 1000 Hz with two transducers that fulfill the requirements was also tested. It was then decided to use these two sensors at their respective maximum sampling rate to measure the variables for the experiment.

Figure 16: PASCO Universal Interface (left) and two sensors (right).

3.1.6 Miscellaneous items

Capillary tube: This experiment requires the use of a capillary tube through which air is injected to form bubbles inside the fluid to be analyzed. A glass pipette was chosen, one end was connected to the air source and the other end was submerged. Measurements of its diameter are discussed on the Chapter 4.

Hoses: In order to transport the air from the source to the pipette and the pressure sensors, it was necessary to assembly a set of hoses. The PASPORT sensors came with a set of hoses that were used on this experiment. To attach the hoses between them, metal joints were tested but the seal was not good enough and there were some air leakages that were verified using soap foam. For this reason, they were replaced by plastic unions and the problem was solved.

3.2 Experimental Setup

Once all the elements of the equipment have been selected, the next step is to continue with the assembly. A diagram of the equipment setup is shown in the Figure 17. A detailed description of this and the configuration parameters are discussed in the following sections.

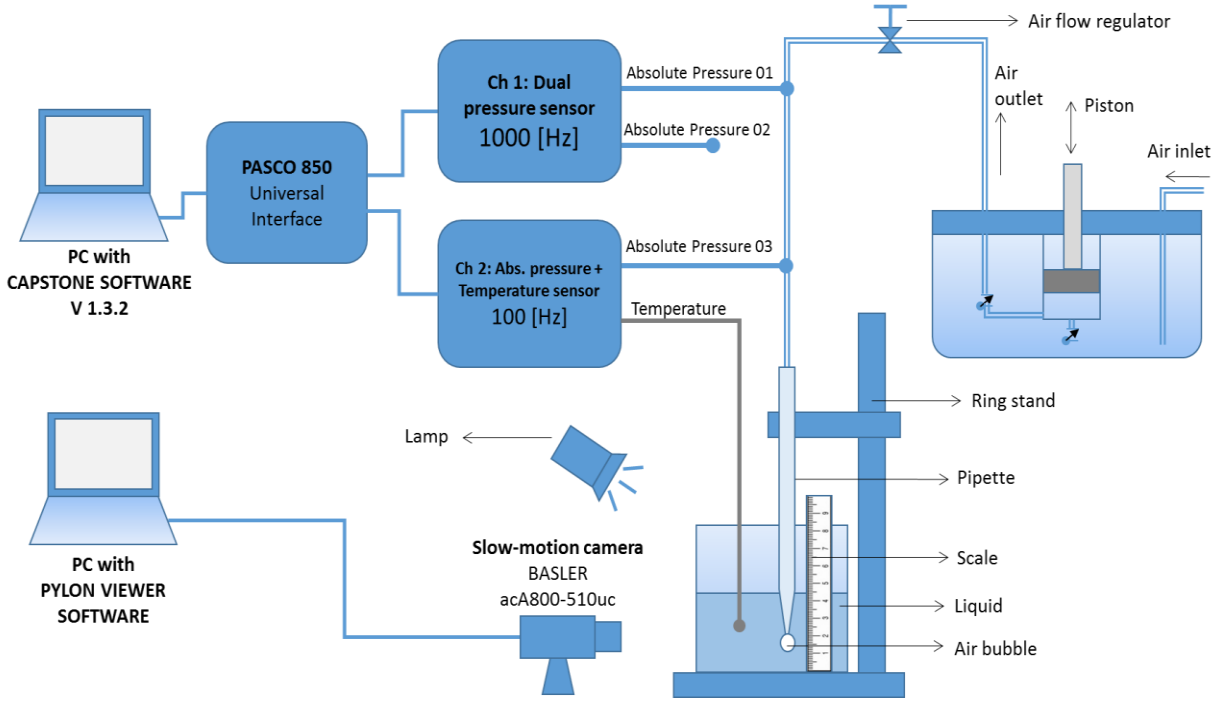

Figure 17: Equipment setup.

3.2.1 Experiment assembly and configuration parameters.

Pneumatic loop: The hoses were connected according to the schematic drawing shown on Figure 18. It can be seen that two derivations were considered for the pressure sensors. In the hose attached to the air source, a squeeze off tool was installed to control the flowrate of air. In order to hold the pipette, a ring stand with a moving clamp was used to modify the immersion depth of the pipette inside the fluid. A caliper was used to measure this length.

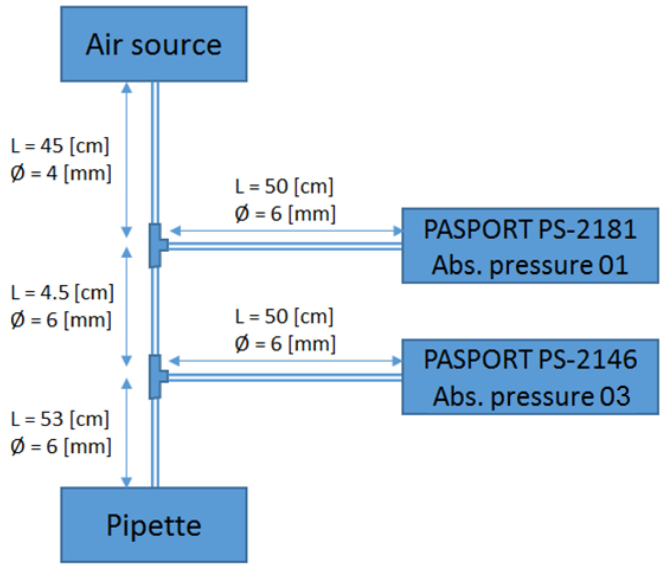

Figure 18: Hoses layout.
The dimensions are shown.

Pressure and temperature measurement: As mentioned, there are two PASPORT sensors that will be used in this experiment. These will perform the measurements of pressure and temperature. Prior to running the experiment, all the configuration was done by the use of the software PASCO Capstone version 1.3.2.

- Referring to Figure 17, the Dual Pressure Sensor (PS-2181) has two pressure transducers to measure differential pressure, one of this is connected to measure the pressure from the air source (absolute pressure 01) and the other is left open to measure the atmospheric pressure (absolute pressure 02). The maximum sampling rate of 1000 Hz with a resolution of 3.5 Pa was set.
- The second sensor, the Absolute Pressure Temperature Sensor (PS-2146) has a transducer port connected to measure the absolute pressure from the air source (absolute pressure 03). The other port is connected to a temperature probe to measure the temperature of the fluid to be analyzed. This sensor was configured at its maximum sampling rate of 100 Hz with a resolution of 2 Pa for the pressure sensor and 0.001 ˚C for the temperature sensor.

Camera: The image acquisition process of bubble formation is assured by the camera which was placed at approximately 6 cm form the tip of the pipette and perpendicular to the wall of the cube, as seen on Figure 17. To perform measurements, a transparent scale was placed in a vertical position next to the pipette in a scale 4:1. This means that every four lines from the

scale is one millimeter. The lamp was placed at 30 cm from the cube at an angle of 5˚ from the view line of the camera. A white background was placed behind the cube to improve the image quality. Regarding the configuration of the camera, it was set with a resolution of 512 x 600 pixel, an exposure value of 59 microseconds and an acquisition rate of 500 fps. The software used to perform this was Pylon Viewer, version 5.0.11.10913 64-Bit.

Fluids: As it was already mentioned, the surface tension will be measured in five different fluids. The plastic cube will be filled with approximately 260 [cm^3], obtaining a level of 6 cm measured from the bottom that will give access to perform measurements at different depths.

As seen in Table 2; Water, n-Hexane and n-Octane will be used without diluting them. For the solutions of ethanol at 10%w and 30%w it will be necessary to perform some calculations with the purpose of having the exact amounts of alcohol and water to be mixed. The ethanol available on the laboratory came with a solution of 97%. The calculations are shown below by using basic principles of mass balance and the results are shown in the Table 3.

1. To obtain 300 g of ethanol solution at 10%w:

   Weight of ethanol solution 97%w:

$$\frac{300\ [g_{\ SLN\ 10\%}]}{1} * \frac{10\ [g_{\ 100\%ethanol}]}{100\ [g_{\ SLN\ 10\%}]} * \frac{100\ [g_{\ SLN\ 97\%}]}{97\ [g_{\ 100\%ethanol}]} = 30.928\ [g_{\ SLN\ 97\%}]$$

   Weight of water:

$$\frac{300\ [g_{\ SLN\ 10\%}]}{1} * \frac{90\ [g_{\ H2O}]}{100\ [g_{\ SLN\ 10\%}]} - \frac{30.928\ [g_{\ SLN\ 97\%}]}{1} * \frac{3\ [g_{\ H2O}]}{100\ [g_{\ SLN\ 97\%}]} = 269.072\ [g_{\ H2O}]$$

2. To obtain 300 g of ethanol solution at 30%w:

   Weight of ethanol solution 97%w:

$$\frac{300\ [g_{\ SLN\ 30\%}]}{1} * \frac{30\ [g_{\ 100\%ethanol}]}{100\ [g_{\ SLN\ 30\%}]} * \frac{100\ [g_{\ SLN\ 97\%}]}{97\ [g_{\ 100\%ethanol}]} = 92.784\ [g_{\ SLN\ 97\%}]$$

   Weight of water:

$$\frac{300\ [g_{\ SLN\ 30\%}]}{1} * \frac{70\ [g_{\ H2O}]}{100\ [g_{\ SLN\ 30\%}]} - \frac{92.784\ [g_{\ SLN\ 97\%}]}{1} * \frac{3\ [g_{\ H2O}]}{100\ [g_{\ SLN\ 97\%}]} = 207.216\ [g_{\ H2O}]$$

Table 3: Quantities to be mixed for different concentrations of ethanol.

Fluid	Quantities for solution of ethanol 10%w, g	Quantities for solution of ethanol 30%w, g
Water	269.072	207.216
Solution of ethanol (97%w)	30.928	92.784
Total	*300*	*300*

3.3 Experimental Method

Once all of the equipment was assembled according to Figure 17 and Figure 18, and configured according to the parameters established in Section 3.2, the next step is to start the experiment, validate the measurements and finally establish the value of surface tension. According to the theory presented in Section 2.4.1, the normal approach to calculate the surface tension is limited to a defined range of capillary radius and immersion depths. For this reason, the approach that will be used is mentioned in Section 2.4.2, where there are no limitations of capillary radius. However, it is necessary to perform measurements in different depths and perform a linear regression. It is therefore of special interest to verify the accuracy of this method in fluids with different values of surface tension.

3.3.1 Data acquisition

To start the experiment, the capillary tube is carefully lowered inside the cube until the tip touches the liquid. This depth is recorded by measuring the distance between the moving clamp and the top of the ring stand. This serves as the reference level. The piston from the bottletop dispenser is lifted to generated air flow and is regulated by the use of the squeeze tool until approximately one bubble per second is observed. Once the airflow stopped because the piston has reached its lowest position, it is time to proceed with the image and sensor logging.

With no airflow, the recording from the PASCO and the camera are activated manually at the same time to record a period of time of around 3 seconds. Then, the piston is lifted to generate airflow for another 7 seconds. Finally, the image and sensor acquisition are stopped after being registering information for around 10 seconds. This data will be used to perform

noise analysis and image processing. After analyzing and validating the data, the value of surface tension for each fluid will be calculated.

After the previous step the moving clamp is lowered 2 mm approximately. This length is carefully measured with a caliper in order to have an accurate value of the capillary depth. The process is repeated again for this new depth. A total of 11 different depths were performed for each fluid.

3.3.2 Importing data

The data recorded by the PASCO software is in a .txt format. The signals generated by the Dual Pressure Sensor has a sampling rate of 1000 readings per second, and the Absolute Pressure Temperature Sensor 100 readings per second. A script in Matlab was developed to import the data to vectors. This script is presented on the Appendix A1.

The nomenclature for the vectors was established as follows:

Time = Time vector.

CH1AbsP1 = 1^{st} absolute pressure reading from Dual Pressure Sensor.

CH1AbsP2 = 2^{nd} absolute pressure reading from Dual Pressure Sensor.

CH1DeltaP = Difference between absolute pressure readings from Dual Pressure Sensor.

CH2AbsP = 3^{th} absolute pressure reading from Absolute Pressure Temperature Sensor.

CH2Temp = Temperature reading from Absolute Pressure Temperature Sensor.

3.3.3 Noise analysis

Before starting the calculations, it is necessary to analyze and validate the data. This is crucial because the pressure and temperature recordings can be infected by noise or unwanted signals that in some way can affect the results from the test. For this reason, a noise analysis is performed in the signals of pressure and temperature generated by the sensors. With the use of Matlab, script was developed to perform these analyses.

As mentioned in the theory presented in the section 2.5, three main analyses are performed:

Fast Fourier Transform (FFT): This analysis is based in defining a signal over a period of time and run the FFT code to divide this signal into its frequency components, as shown in the Figure 10 and discussed in section 2.5.1. The Matlab script is presented in the Appendix A2. Because three time intervals can be defined, analyzes of the signals will be carried out in different sections in order to identify predominant frequencies that may interfere with the variables that will be measured. The first interval is before starting the experiment to identify possible noises that are not linked to the experiment itself. The second interval is between the pressure peaks when the bubbles are released with the intention to identify noise linked to the experiment but not affected by the sudden expansion of the bubbles. The third interval is considering the whole signal where is observed a typical saw tooth pulse.

Low Pass Filter: As discussed in section 2.5.2, a cutoff frequency Wc is established. The signals with a frequency higher than this value will be attenuated while the rest of the signal is not affected. It should be noticed that a high value of Wc not only attenuates the noise but also the pressure signal. To implement this in Matlab, it was necessary to create a function of the LPF and use this in another script. These codes are presented in the Appendix A3.

Moving average filter: A parameter *n* is defined as the value of the samples that will be averaged according to the theory presented in section 2.5.3. The implementation of this code in Matlab is presented in the Appendix A4.

It is of special interest to apply the filters in such way that the signal doesn't show noise but the pressure peaks before a sudden change is identified.

These scripts were developed with the help of Prof. Rune Time, Herimonja A. Rabenjafimanantsoa and Dan Sui.

3.3.4 Image processing

Once the images were acquired, it is necessary to perform the analysis of them. With the use of Matlab, there are two main analyses that were performed.

The first analysis consists of the measurement of the radius of the bubble. According to theory and shown in Figure 8, the maximum pressure will be the moment when the bubble has its minimum radius. After this point, the bubble suddenly expands on the tip of the capillary tube and is released. In all the images there is a transparent scale that will be used to perform length measurements. In this case the value needed to perform the surface tension

calculation is the minimum radius just before the bubble expands that is equal to the radius of the capillary tube. The image of this moment is analyzed by counting the number of pixels of the radius. Since there is a scale, it is easy to calculate the length per pixel and then the radius. This analysis will be done in each fluid and in each depth of the capillary tube.

The second analysis is to study the movement of the interface between the water and air. An algorithm in Matlab was developed by Prof. Rune Time that can be found in the Appendix A5. This code is based on the following:

- Convert each image to a gray scale, this assigns a value between 000 and 255 to each pixel in the image. A value of 000 means totally black while 255 means white, intermediate values represent a grayscale.
- A set point is selected in the range mentioned before, for example 120.
- A vertical line is chosen. All the pixels above the value of the set point are assigned to a "true" value, and the values below this set point receive a "false" value. An example of this can be seen clearly in the Figure 19 where the upper figure is the image taken by the camera. The red, blue and black lines show clearly the variation of the grayscale due to the marks on the meter stick. The lower figure shows only the lines considering the x-axis as length. This is in concordance with the values of the meter stick.

With this code it is possible to analyze how the interface moves along the capillary tube because there is a variation on the gray intensity in this point. Let's consider the cylinder formed by the inner hole of the capillary tube. If we set an imaginary vertical line just on the external part and another vertical line on the center, it is possible to determine how the curvature of the meniscus is formed since the starting point is a near flat interface that curves along the time while injecting air. In addition, by measuring the distance from the top of the image to the interface, it is possible to determine the position of this interface along the time if we perform the analysis in all the images. This can be understood in a better way in Chapter 4 where the results of these analyses are shown.

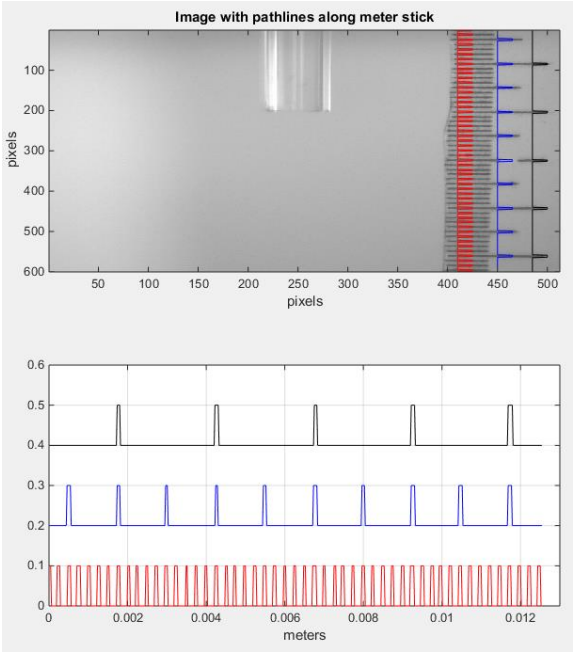

Figure 19: Image with pathlines along meter stick

3.3.5 Surface tension calculation

In order to perform the calculation of the surface tension, the equation (7) will be used:

$$\Delta P_{MAX} = \frac{2 \cdot \sigma}{r} + \beta \cdot h_A \cdot \rho_A \cdot g \qquad (7)$$

By performing a plot of ΔP_{MAX} vs h_A from experimental data and making a linear regression of the form $Y=mx+b$, the parameter β and $\frac{2 \cdot \sigma}{r}$ can be calculated [8]. In this case, $(\beta \cdot \rho_A \cdot g)$ will correspond to the slope of the line which is m, and $\frac{2 \cdot \sigma}{r}$ will correspond to the intersection between the Y axis and the regression line which is b. The other parameters are obtained as follows:

- The value of ΔP_{MAX} is the difference between the atmospheric pressure and the maximum pressure recorded. This value will be read from the plots after performing the noise analysis and applying the LPF and MAF filters.
- The value of bubble radius r will be obtained from the first analysis on the image processing.
- h_A is recorded during the experiment with a caliper.
- ρ_A, the density of the fluid for a given temperature, it is obtained from literature.

- g is the value of gravity acceleration.

The temperature will be obtained by averaging the values recorded during the experiment for each fluid since the principle of the experiment is based on constant temperature.

Once the values of surface tension are obtained, it is necessary to compare them with values from literature. These values are presented in Table 2 for different temperatures. According to Figure 1, the values of surface tension for small variations in temperature show a linear behavior and will be obtained by interpolation.

Chapter 4

4. Results and discussions

As it was discussed in the previous chapter, the recorded data to perform the analysis of the surface tension by the Maximum Bubble Pressure Method (MBPM) was done with the help of sensors to measure absolute pressure and temperature, and a slow-motion camera to capture images while the bubbles are forming on the tip of the capillary tube. These data will be presented and discussed in this section by analyzing them using mathematical filters and image processing. Once the data is validated, the surface tension is calculated and the results are discussed.

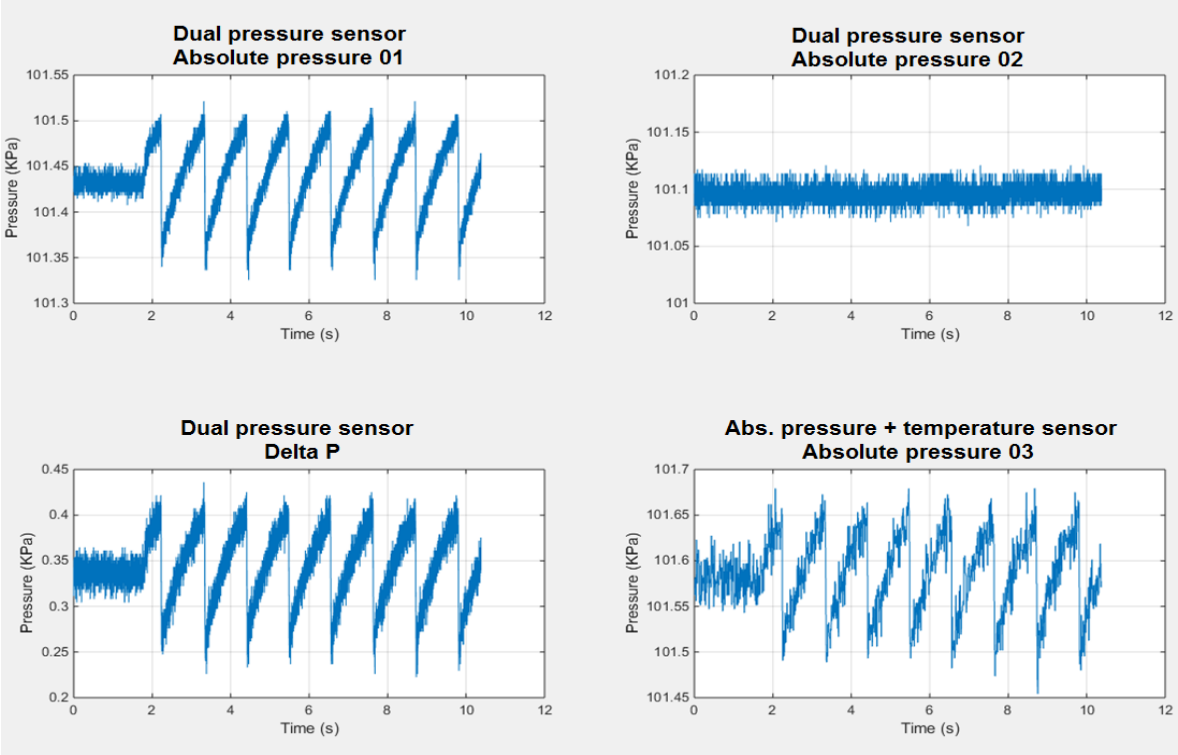

Figure 20: Pressure readings with ethanol 10%w at 23.08 mm

The raw data registered by the PASCO and its sensors needs to be analyzed before proceed with further calculations. Figure 20 shows plots of the data recorded in ethanol 10%w at 23.08 mm with the pressure transducers as function of time: two readings from the Dual Pressure Sensor and its delta P, and one reading from the Absolute Pressure Temperature Sensor.

Additionally, Figure 21 shows a plot of the temperature readings as a function of time with the Absolute Pressure Temperature Sensor associated with the previous pressure readings. It was expected to obtain a constant value of temperature. A more detailed analysis regarding this topic is presented in Section 4.1.

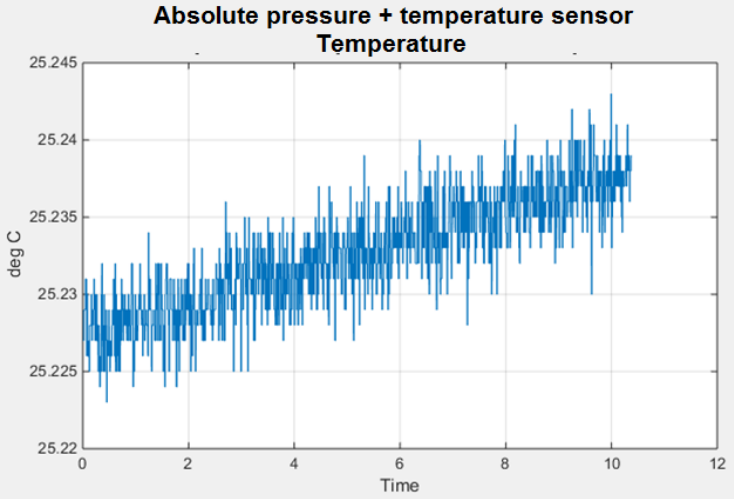

Figure 21: Temperature readings with ethanol 10%w at 23.08 mm

In Figure 20, the plots shown are consistent with the information presented in the theory chapter regarding the principles of the MBPM. There is a pressure buildup while the bubble is in formation inside and on the tip of the capillary until a maximum value is reached. At this point the bubble is released and the pressure drops quickly to start a new cycle. It can also be seen that the data presents some low frequency fluctuations. For this reason a noise analysis will be performed in Section 4.2 to validate the data.

Once the images are captured, it necessary to perform an analysis of them in concordance to the theory and the procedure described on the experimental method. These images will be linked to the data recorded by the pressure sensors. This discussion is presented in the Section 4.3.

Finally in Section 4.4, with all the information obtained from the previous procedures, the surface tension is calculated and compared with the values presented in Table 2.

It is necessary to emphasize that the shapes of the curves are similar in all the experiments but they only vary in magnitude. In the next Sections one experiment will be used to illustrate the analysis.

4.1 Temperature increase analysis

Inside the data obtained from the temperature measurements, it was seen that the temperature has a trend to increase along the time at a rate of approximately 0.01 ˚C per every 10 seconds according to Figure 21. Similar behavior was seen in all the experiments. Even though the increase is minimal inside the period were the measurements were taken, it is necessary to determine if the bubbles influence the increase in the temperature of the fluid or if it is mainly because of the heat generated by the lights used to illuminate the experiment.

To perform this, the same initial layout of the equipment was used. Two scenarios were proposed: 1) No bubbles generated, and 2) Injecting air to produce bubbles. It should be noted that the conditions of the light were identical for both of the experiments mentioned above. The fluid used is distilled water.

In order to make a fair comparison it is necessary that both scenarios must start at the same temperature and at same room temperature conditions. At the beginning of the experiment the temperature sensor is left out of the water for 5 minutes to record the environment temperature and submerged into the water afterwards for 30 minutes to record the temperature for each experiment. The recordings of temperature can be seen on Figure 22.

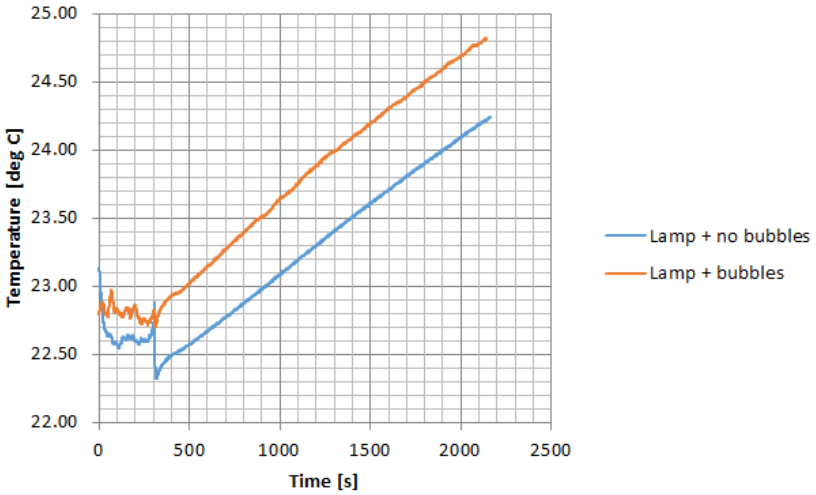

Figure 22: Plot of the data from the temperature increase analysis

Since it was not possible to start the experiment at the same conditions due to small variations in the room and water temperature, it was decided to use the values once no quick variations were observed. From Figure 22 when both systems have reached a temperature of 23 ˚C there

are no abrupt variations. Hence this will be considered t=0 s when performing the analysis. With this, we ensure that the starting points for the experiments are the same. In Figure 23 the temperature measurements are shown considering the parameters mentioned above, it is also included the difference between the values.

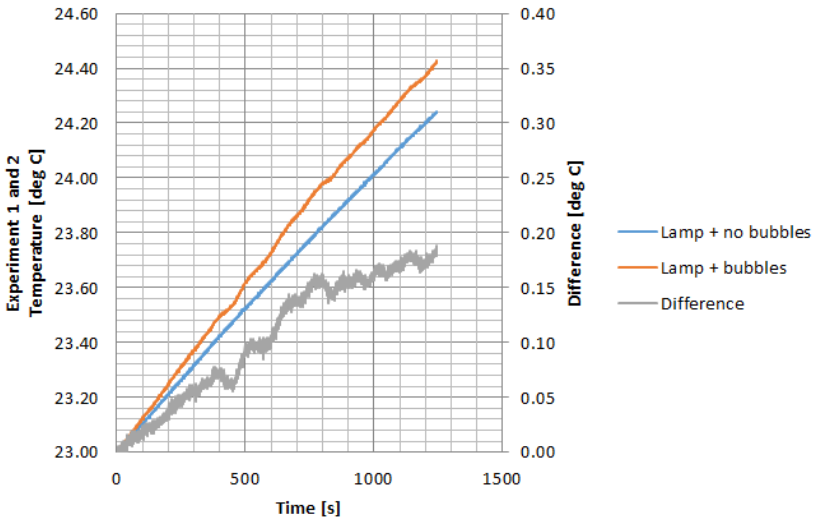

Figure 23: Temperature analysis considering the same starting point for the experiments.

It can be seen that the system where the bubbles were injected reached a temperature of 24.425 ˚C after 1245 s, this means a rate of 0.0114 ˚C every 10 s approximately. In the second system were the bubbles were not injected, a temperature of 24.238 ˚C was reached with a rate of 0.0099 ˚C every 10 s. Based on these results, the following can be said:

- The bubbles help to increase the temperature of the system.
- The expansion of the bubbles can be considered as an adiabatic process (no heat exchange to the system) due to the small size and the very short time while a bubble is traveling from the tip of the pipette to the surface.
- Once a bubble is released, it generates some turbulences and movement of the particles inside the liquid. This movement helps to homogenize the heat distribution inside the liquid and the temperature is increased. A detailed analysis of this phenomenon is out of the scope of the present work.
- The temperature increase during the 11 experiments for each fluid is in concordance to the values obtained in this temperature analysis with an approximate of 0.01 ˚C every 10 s.

Since the surface tension is a function of temperature, the value considered will be the average of the readings from the temperature sensor. One value of temperature will be used for each fluid. Between each experiment, the light was turned off to avoid too much temperature increase.

4.2 Noise analysis

Once the theory of noise analysis was considered in the developing of Matlab codes, it is time to apply them in the data that has been recorded. In this section the results after applying these filters will be discussed.

4.2.1 Low pass filter

To exemplify the analysis that was done using the low pass filter, it was decided to use n-Octane and the capillary at a depth of 10.04 mm. Since the plots of the raw data have a similar shape in all the experiments, it is enough to explain only this case. The filtering technique will be similar in all the scenarios since the equipment used and the conditions were the same.

It is necessary to establish the cutoff frequency *Wc* to apply this filter. Three values were evaluated on the pressure data: $Wc = 5$, $Wc = 10$ and $Wc = 40$.

Figure 24 shows the pressure data before filtering and after applying the LPF with a $Wc = 5$ which is the lowest value analyzed. It can be seen that the filtering of the signal is poor. It is still noisy and is difficult to establish the real value of the pressure peaks that will be used in the surface tension calculations.

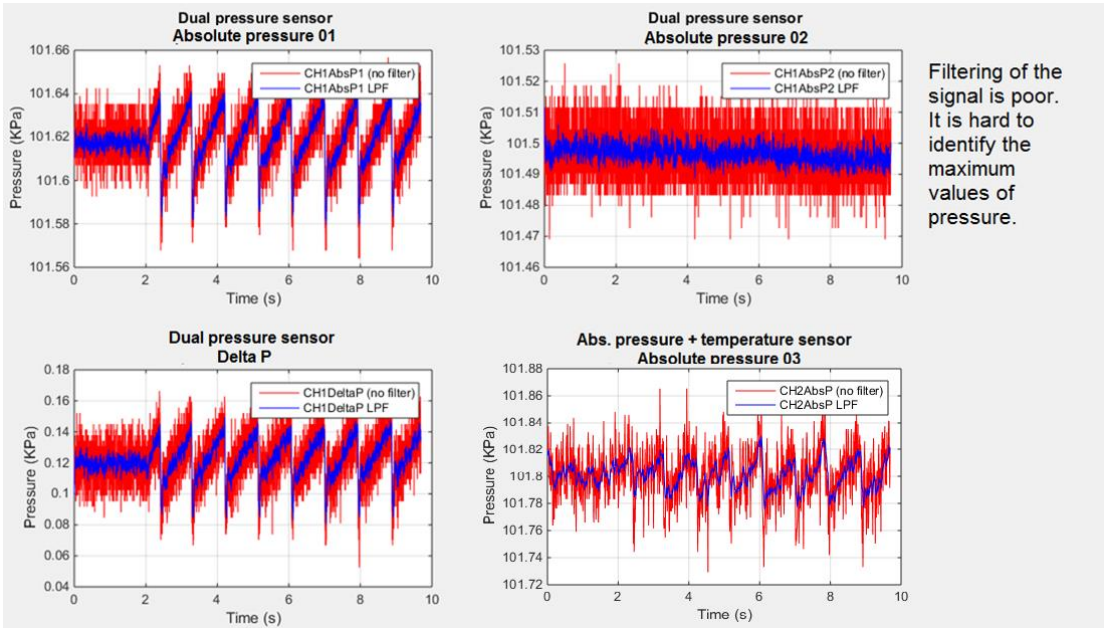

Figure 24: Signal before and after LPF, cutout frequency Wc = 5

In Figure 25, the value of *Wc* = 10 is used. The signal is less noisy and the pressure peaks can be identified. Despite of this, the only signal that shows no improvement is the absolute pressure 03 measured with the Absolute Pressure Temperature Sensor.

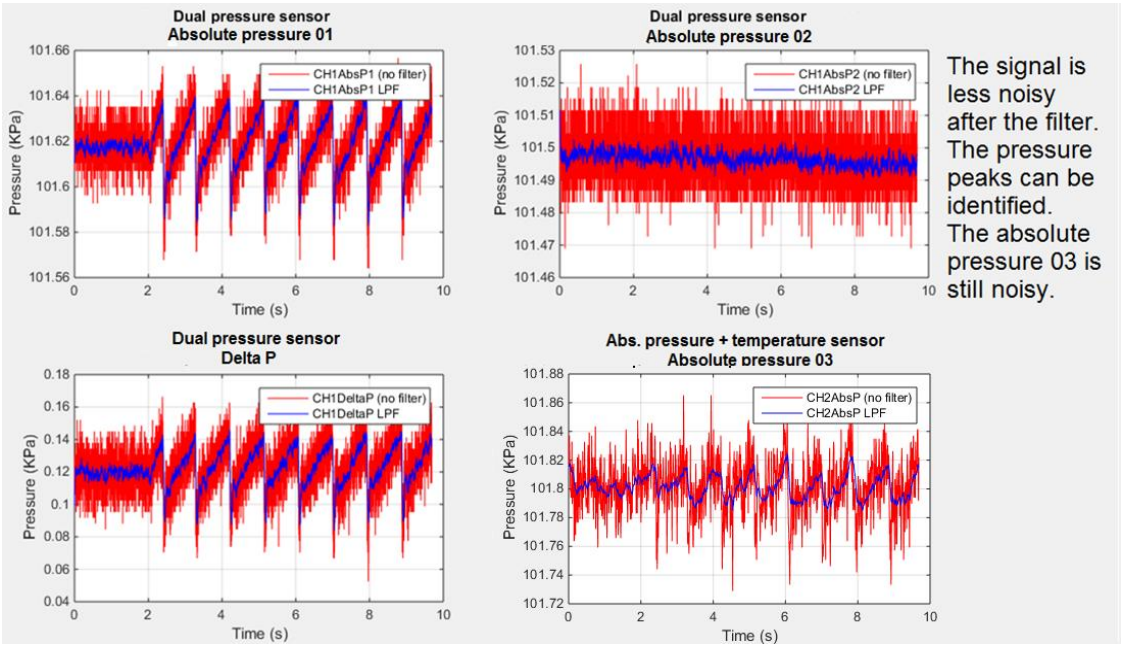

Figure 25: Signal before and after LPF, cutout frequency Wc = 10

Figure 26 shows the raw data and the filtered data with *Wc* = 40. After performing this LPF, the signal is smooth but some valuable information related to the pressure peaks has been lost. On the other hand, the absolute pressure 03 measured with the Absolute Pressure Temperature Sensor is still noisy even after applying the filter and shows poor improvement on the quality of the signal.

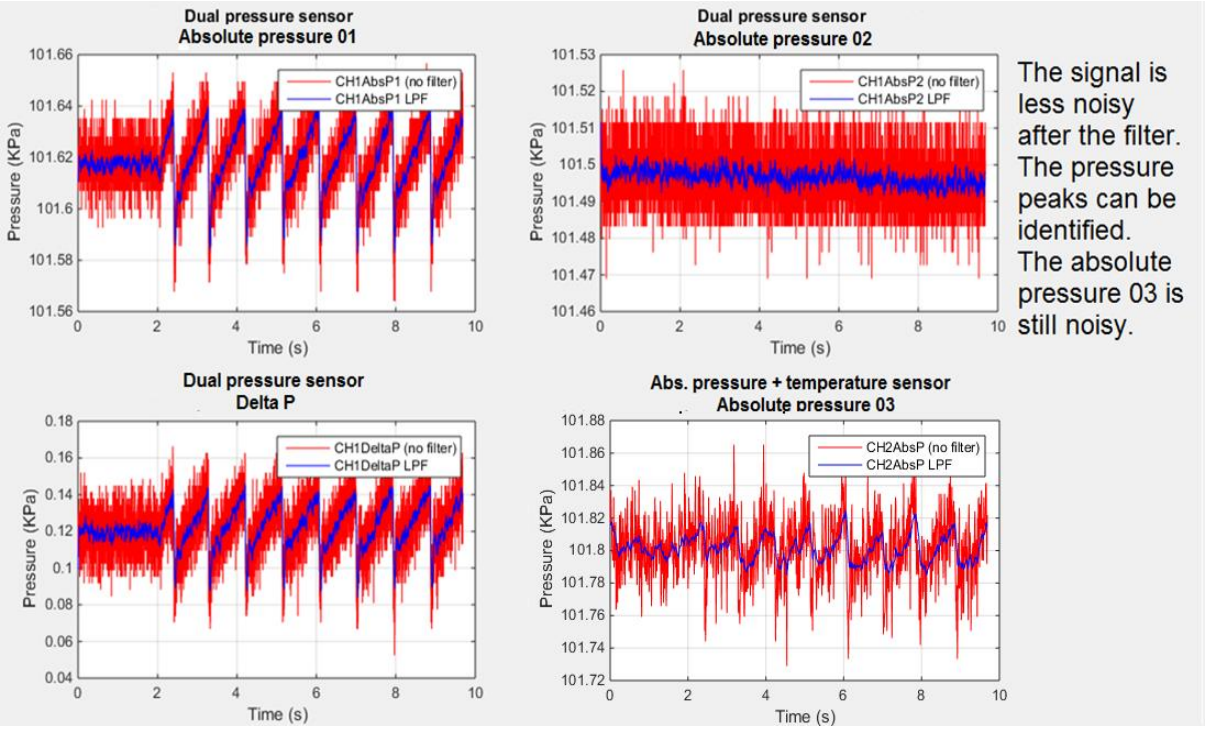

Figure 26: Signal before and after LPF, cutout frequency Wc = 40

To perform the calculations of surface tension, it is necessary to identify pressure peaks on the ΔP signal. It was decided to use the value of *Wc* = 10 for the LPF. The pressure readings performed with the Absolute Pressure Temperature Sensor show no improvement after applying this filtering technique. The noise associated could not be decreased. This is not the case of the Dual Pressure Sensor where the filter works adequately.

4.2.2 Moving average filter

Since the moving average filter (MAF) is considered as a LPF, the scenario will be identical as the one shown in Section 4.2.1. The fluid is n-Octane and the capillary at a depth of 10.04 mm. This case will be analyzed as an example for all the experiments.

As mentioned in the theory chapter, it is necessary to establish values of *n* (samples to be averaged) to perform the analysis. Three values were chosen: *n* = 8, *n* = 20 and *n* = 50.

Figure 27 shows the signal after applying the MAF with *n* = 8. It can be seen that the filtering is poor and the data is still noisy. The absolute pressure 03 from the Absolute Pressure Temperature Sensor shows no improvement on the data quality.

Figure 28 considers a parameter of *n* = 20. The quality of the data after the MAF has been improved, the pressure peaks can be seen easily compared with a lower value of *n*, but the signal from the Absolute Pressure Temperature Sensor (absolute pressure 03) is still noisy.

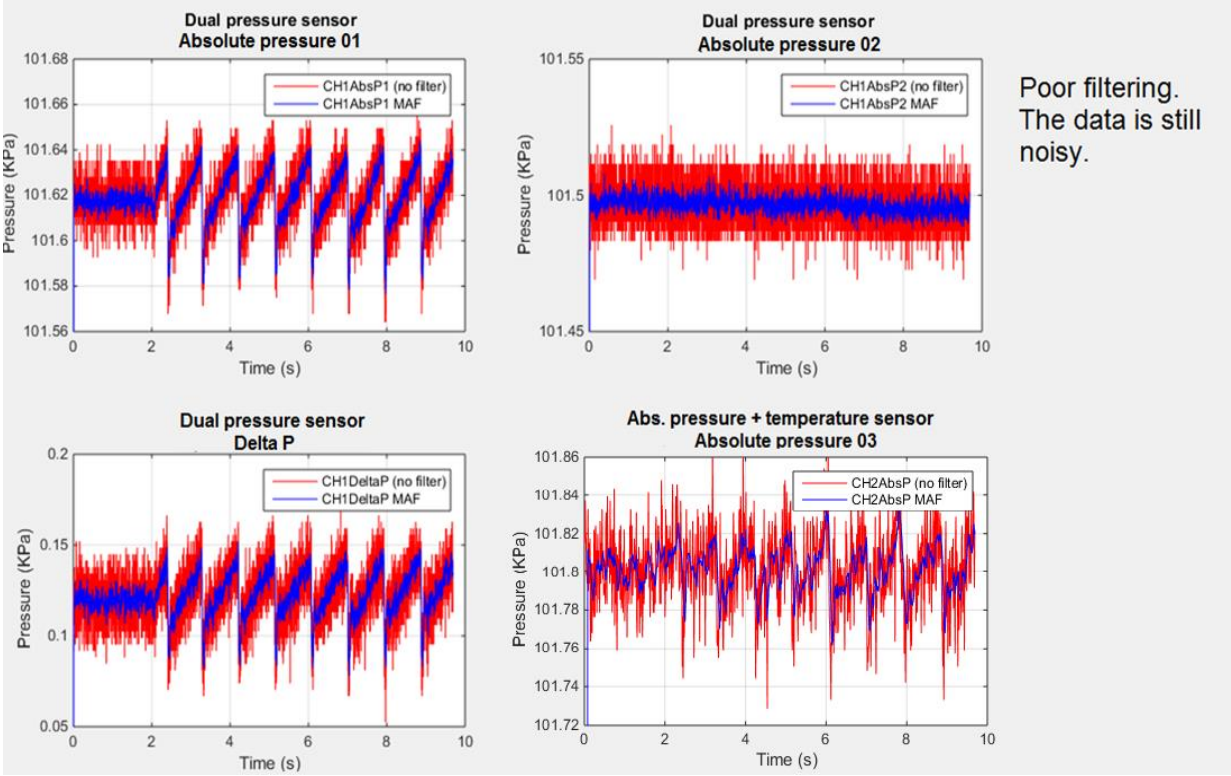

Figure 27: Signal before and after MAF, samples averaged n = 8.

A large value of *n* is considered in Figure 29, with *n* = 50. The signal obtained after the filter is smooth but the pressure peaks have decreased compared with the previous case, this can lead to lower readings of the real value of the pressure. The signal from the Absolute Pressure Temperature Sensor shows almost no improvement in the quality.

After this analysis, it was decided to use a value of *n* = 20. Similar to the LPF case, only the absolute pressure 03 signal from the Absolute Pressure Temperature Sensor could not be

improved by implementing a MAF because in all the analyzed cases the output signal is noisy.

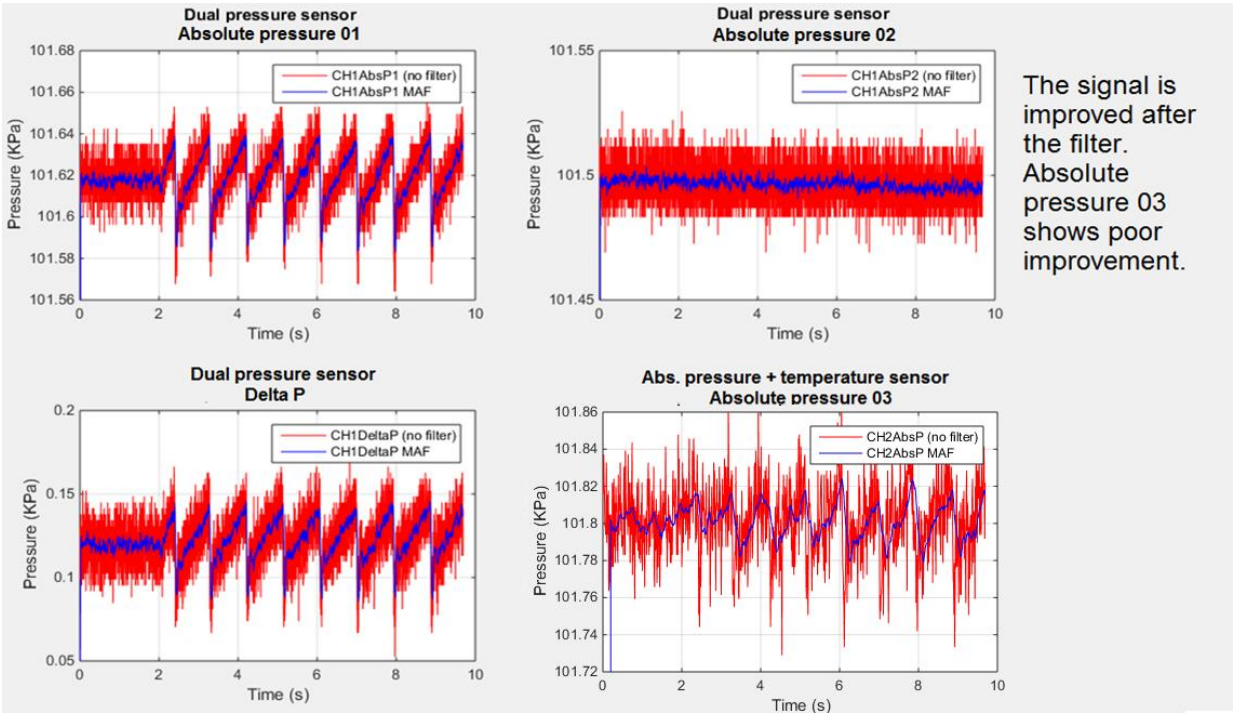

Figure 28: Signal before and after MAF, samples averaged n = 20.

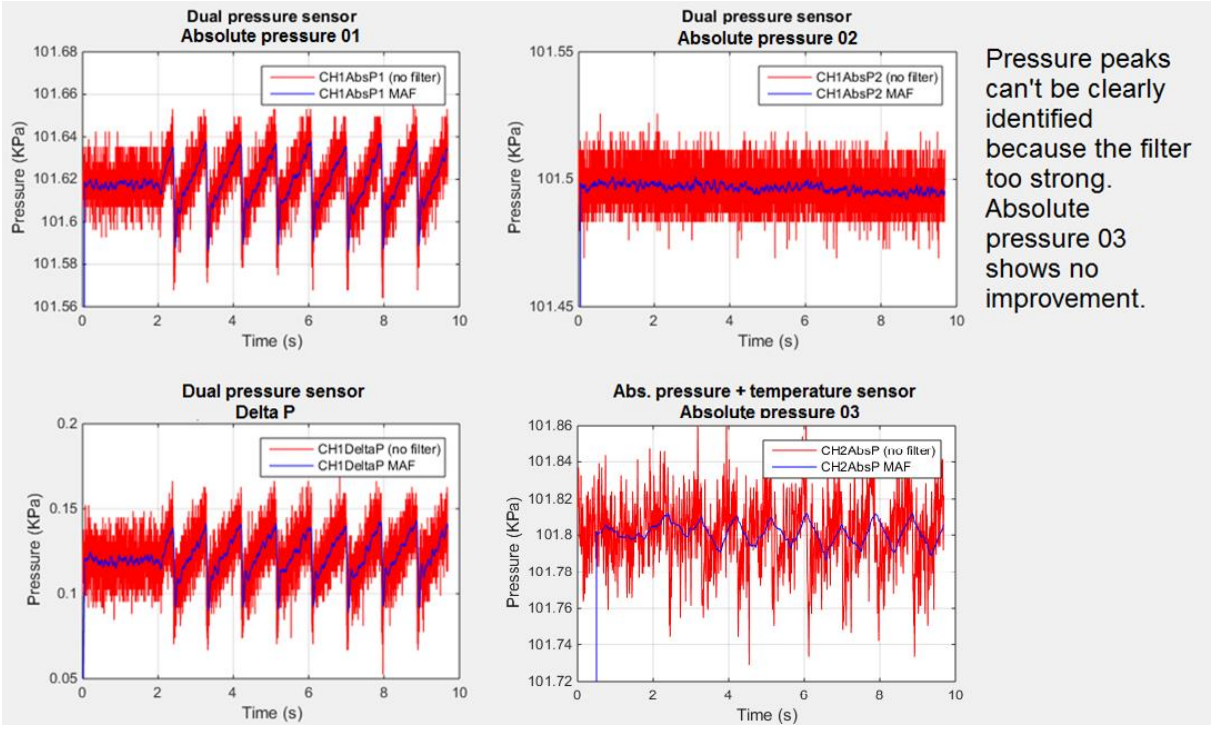

Figure 29: Signal before and after MAF, samples averaged n = 50.

4.2.3 Fast Fourier transform

As it was already discussed in the theory section, the Fast Fourier transform (FFT) can be applied to any interval of the signal in order to identify predominant frequencies. The fluid chosen for this is n-Octane and the capillary at a depth of 10.04 mm, these are the same conditions from the LPF and MAF analysis.

First analysis

The first analysis was performed on the signal before starting the pumping of air, which corresponds to the first 2 seconds. The FFT was applied in the pressure signal and the results are shown in Figure 30. It can be seen that there is no a predominant frequency in the range from 0 Hz to 500 Hz and the amplitude values are aleatory within a range in the absolute pressure 01, absolute pressure 02 and Delta P. Based on this, it can be said that this is white noise. The FFT from the absolute pressure 03 measured with Absolute Pressure Temperature Sensor shows similar behavior from 0 Hz to 50 Hz, this is because the sampling rate of the sensor is only 100 Hz. Regarding the temperature, the FFT of these data can be seen in Figure 31. The white noise is predominant in the range from 0 Hz to 50 Hz. Note that there is a peak at 50 Hz, this can be linked to noise produced by electric sources at 50 Hz and its magnetic fields.

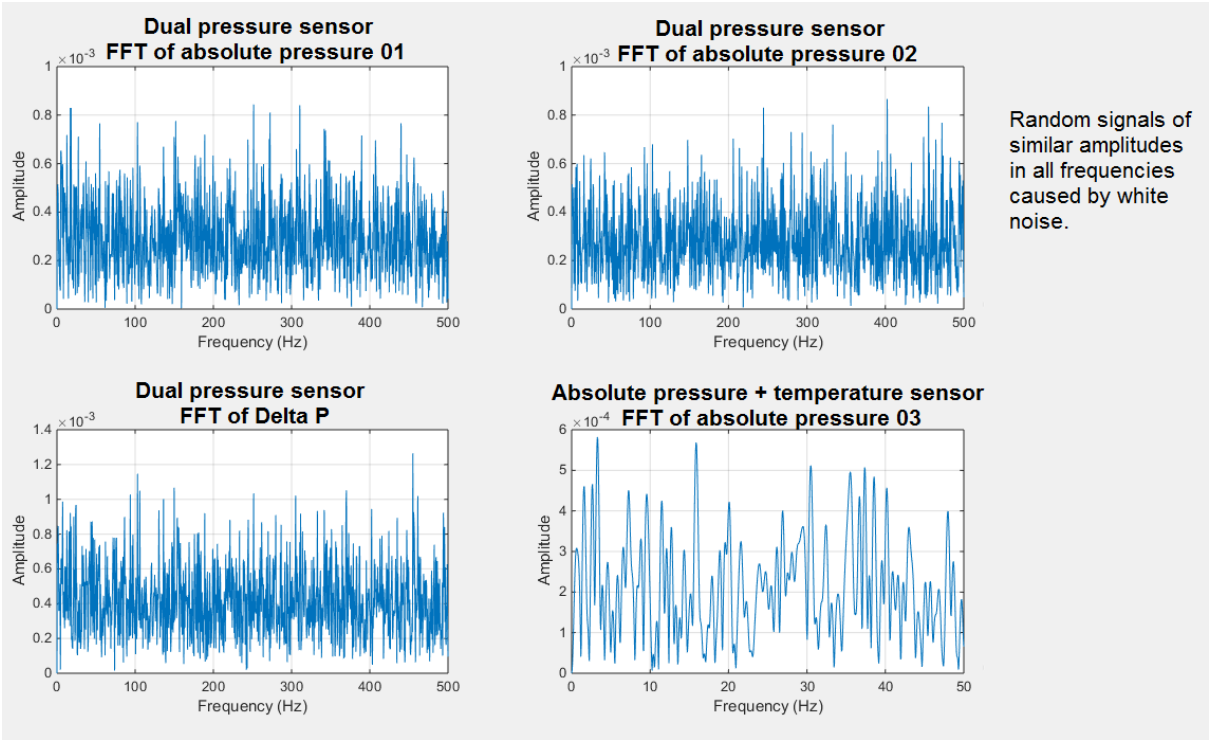

Figure 30: FFT of pressure before starting experiment, the first two seconds

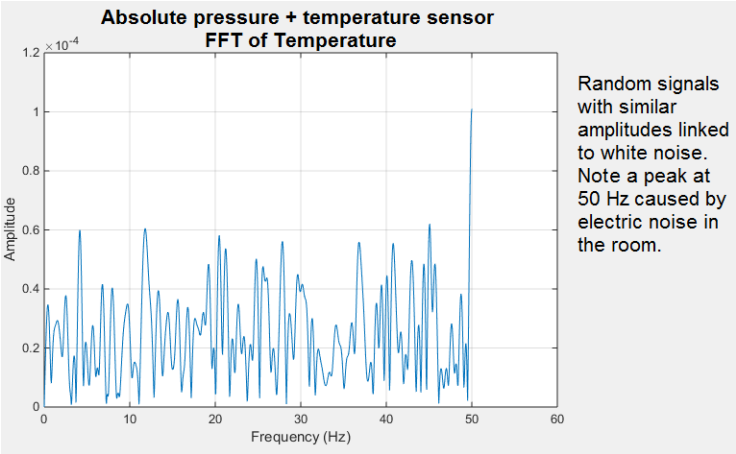

Figure 31: FFT of temperature before starting the experiment

Second analysis

The second analysis was performed in the pressure data with the intention to identify noise linked to the gas-liquid interface change. This study was done in the period between the generation of bubbles in order to identify a possible dominant frequency and avoid the interference caused by the sudden expansion of the bubble. Figure 32 shows a pressure signal in a given time interval (CH1DeltaP (no filter), red line) that is not smooth even after applying the LPF (CH1DeltaP LPF, blue line). This behavior is similar to all the experiments in all intervals. For this reason, the FFT will be used to perform the analysis to identify noises and its frequencies. There are pressure peaks around t1 = 2.45 s and t2 = 3.25 s leaving an interval of 0.8 s approximately. With an acquisition rate of 1000 Hz it leaves around 800 points to perform the analysis.

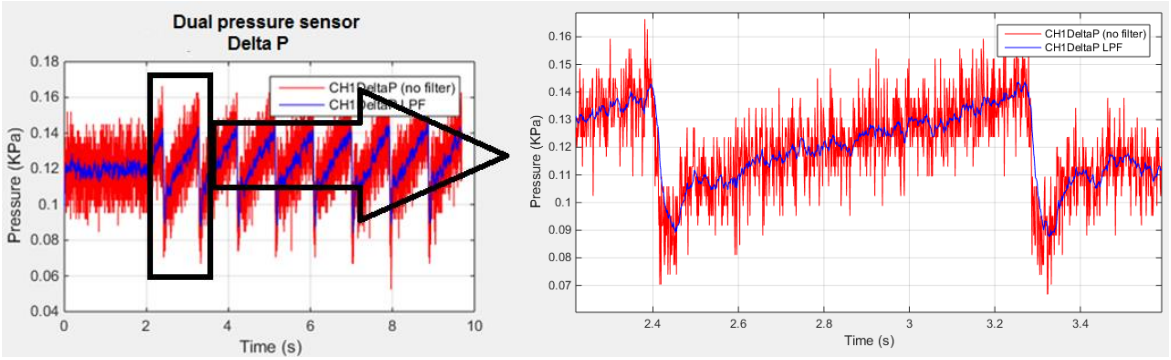

Figure 32: Signal of delta pressure, experiment with n-Octane at a depth of 10.04 mm

Two scenarios are proposed where the input data will be called f(t):

1) Using unfiltered pressure data (CH1DeltaP); and

2) Using filtered pressure data after the LPF (CH1DeltaP LPF).

The data in the analyzed interval seems to show a linear behavior vs. time. For this reason a linear fit was performed and was called y(t). The equation of this line was found by the use of Matlab and was in the form y(t)=y1+k*t by using the Least Square Method where k is the slope of the line. The graph of the results are shown in Figure 33. A new vector g(t) was found by performing the operation g(t)=f(t)-y(t) which shows the difference between the linear fit and the pressure measurements. With this the data is normalized and the FFT can be applied. The results are shown in Figure 34.

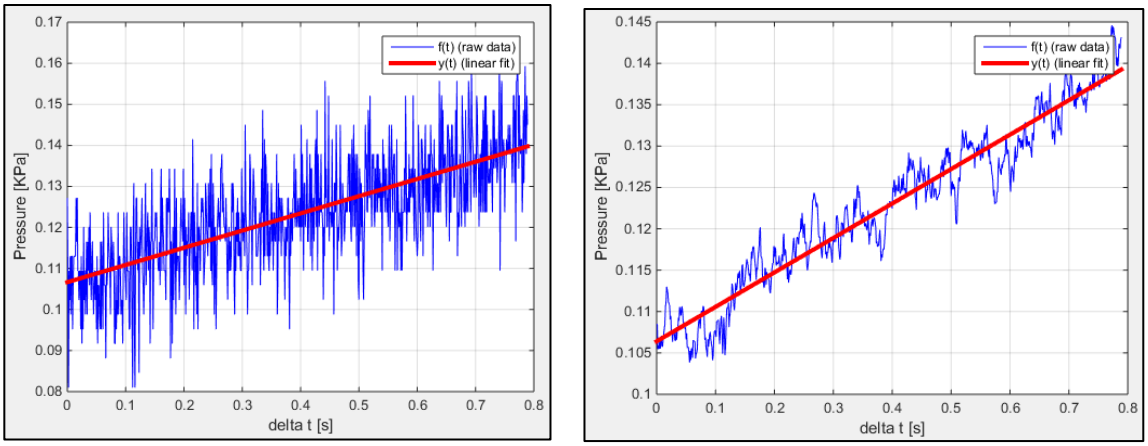

Figure 33: Unfiltered data (blue left), after LPF (blue right) and its corresponding linear fit (red).

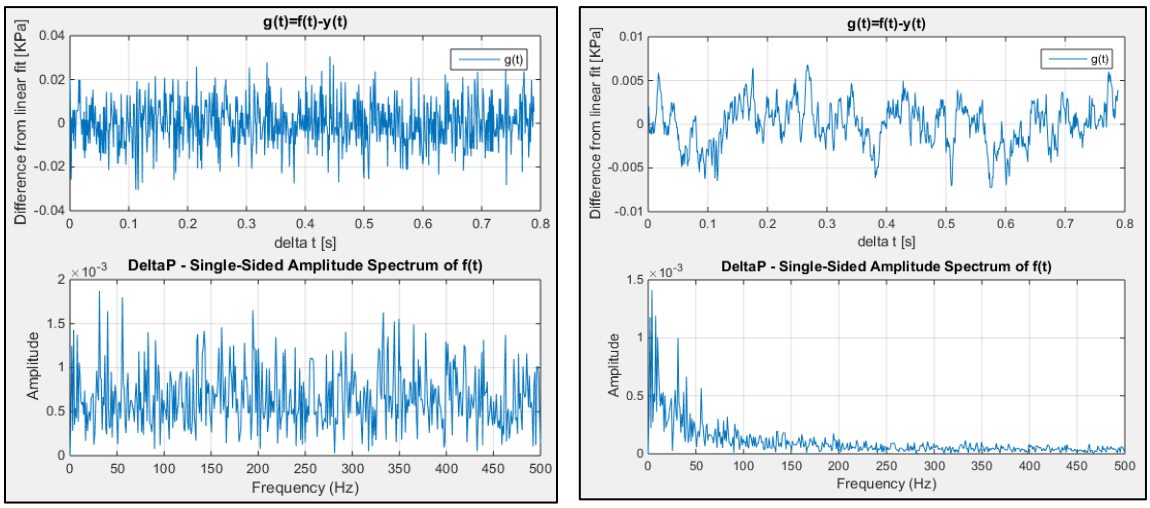

Figure 34: Normalized pressure data g(t) and its FFT, unfiltered data (left) and after LPF (right).

The FFT analysis of the unfiltered data (Figure 34, left) shows many frequencies with similar amplitudes and there is not a dominant frequency. At first glance one could say that is white noise associated to the noise level of the measurement equipment. But there are also another possibilities:

- By analyzing a dynamic system where the interface between gas and liquid is in movement along a glass capillary, the noise can also be related to this movement.
- It should also be considered that the internal surface of the capillary is not uniform and some minor imperfections can lead to changes on the surface wetting which will definitely contribute to the observed behavior.

The FFT of the data after LPF (Figure 34, right) shows that the filter is working adequately. Most of the high frequency signal is decreased and the low frequency signal is present. Similar to the raw data, a random signal can be identified but in this case only at low frequencies because of the LPF.

Third analysis

The third analysis was performed in the whole interval taking into account all data recorded by the sensors. The FFT was applied in the pressure data and the results are shown on Figure 35.

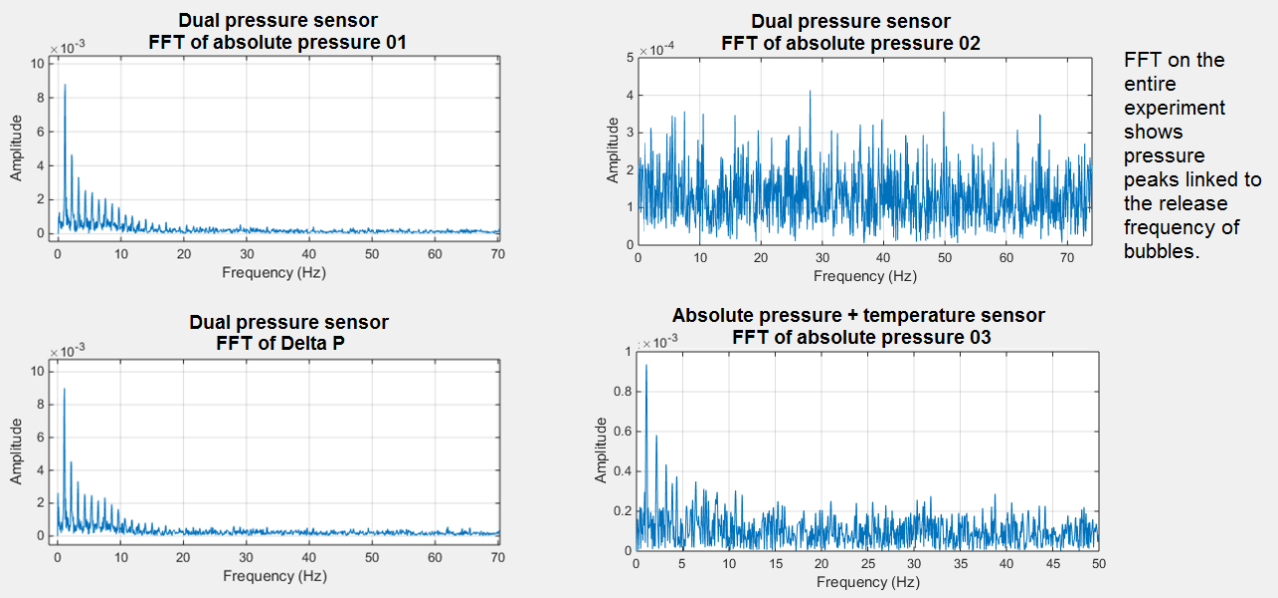

Figure 35: FFT analysis on the pressure data.

The shape of the curve from FFT analysis of the absolute pressure 01 and delta P from the Dual Pressure Sensor is similar. There is a predominant frequency around 1 Hz that is in concordance with the release frequency of the bubbles calibrated for the experiment. As the frequency increases on intervals of 1 Hz, other predominant frequencies are observed with a lower amplitude. This behavior is typically associated to a sawtooth pulse. There are some other small amplitudes along the whole interval that are mainly related to white noise.

The FFT analysis of Dual Pressure Sensor – absolute pressure 02 doesn't show any pulse similar to the other sensors. This is the expected behavior because it was measuring the atmospheric pressure and no big change is probable in this small period of time of 10 seconds. As the previous case, there can be identified multiple small amplitude signals along the whole interval that are associated to white noise.

The FFT analysis from the absolute pressure 03 measured with the Absolute Pressure Temperature Sensor shows a large pulse around 1 Hz but in this case other predominant frequencies related to this pulse can't be identified in higher frequencies typically associated with a sawtooth pulse. The amplitude of the noise is larger than in the previous cases. Similar to the case analyzed with the LPF, this signal is highly affected by the noise at the point that can hinder the pressure signal.

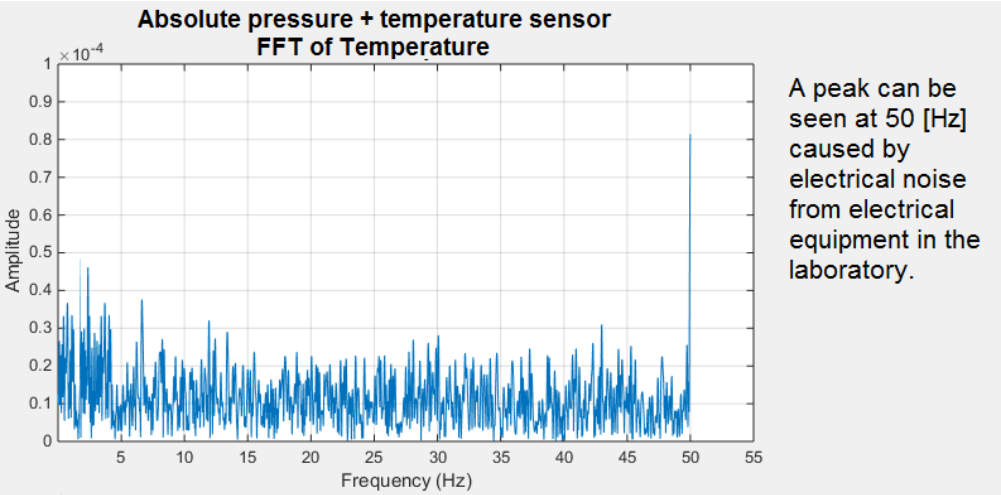

Figure 36: FFT analysis on the temperature data.

Similar analysis was performed on the temperature signal. The FFT analysis can be shown in Figure 36. As seen from the figure, there is a pulse at 50 Hz with large amplitude, this is the frequency of the noise related typically to the electricity in the room. Since this experiment is

carried out in Europe, the frequency of the electricity is 50 Hz. The cable used for the temperature sensor is not shielded and it is very likely that this is the reason why it is so sensitive to electromagnetic fields present in the room.

4.3 Image processing

4.3.1 Radius measurement

With the technique mentioned in Section 3.3.4 the minimum radius of the bubble was measured on images at each depth for each fluid. The results are shown on the Table 4. It can be seen that the measurements are not uniform and the average varies in a range from 0.466 mm to 0.507 mm. At the beginning it was assumed that the cross section of the capillary tube has a circular shape but after these measurements it can be concluded that this is not true. The measurements obtained depend on the position of the camera. It won't be correct to assume that the cross section has an ellipse shape or any other shape without evidence to justify this. Anyway, the ellipse shape will also be analyzed.

Table 4: Radius measurement of the capillary tube

Water		30%w ethanol		10%w ethanol		n-Hexane		n-Octane	
Depth mm	Radius mm	Depth mm	Radius mm	Depth mm	Radius mm	Depth mm	Radius mm	Depth mm	Radius mm
0.20	0.461	0.00	0.494	0.00	0.468	0.00	0.493	0.00	0.501
2.38	0.469	2.18	0.505	2.16	0.469	1.90	0.506	2.14	0.501
4.10	0.469	4.04	0.503	4.18	0.474	4.02	0.502	4.08	0.500
6.24	0.459	6.02	0.504	6.12	0.479	5.86	0.512	6.14	0.500
8.20	0.461	8.10	0.502	8.08	0.476	7.88	0.512	8.12	0.495
10.36	0.471	9.96	0.503	10.16	0.476	9.90	0.500	10.04	0.502
12.38	0.470	12.00	0.503	12.08	0.477	11.90	0.509	12.06	0.499
14.44	0.461	14.02	0.494	14.24	0.472	13.92	0.508	14.04	0.502
16.26	0.463	16.12	0.502	16.14	0.472	15.96	0.510	16.08	0.491
18.40	0.470	17.94	0.501	18.16	0.472	17.84	0.514	18.00	0.503
23.14	0.469	23.00	0.495	23.08	0.470	22.92	0.510	22.92	0.495
Average	**0.466**		**0.500**		**0.473**		**0.507**		**0.499**
Total average		**0.489**							
Standard dev.		**0.018**							

According to the theory presented in Section 2.4, a circular shape with a uniform radius is considered. Otherwise, the calculations became complex and are out of the scope of the

MBPM principles. For this reason, to perform the calculations a circular shape will be considered with a radius equal to the average of all the measurements. It will be expressed with a tolerance that will be the standard deviation of these values. By doing so, the radius is r = 0.489 +/-0.018 mm.

Now an elliptical cross section will be also analyzed and compared with a circular cross section considering the values shown in Table 4. It can be seen form Figure 20 that the ΔP_{max} = 401 Pa.

Considering a circular shape and by the use of the total average radius r = 0.489 mm, the surface tension given by the equation (1) becomes:

$$\sigma = \frac{\Delta P * r}{2} = \frac{401 * 0.489e{-}3}{2} = 98.045 \text{ mN/m}$$

Now, considering an elliptical shape, the value of surface tension is calculated using equation (2). Considering the radii as the minimum and maximum measured, R_1 = 0.466 mm and R_2 = .507 mm.

$$\sigma = \frac{\Delta P}{\left(\frac{1}{R_1}+\frac{1}{R_2}\right)} = \frac{401}{\left(\frac{1}{0.466e{-}3}+\frac{1}{0.507e{-}3}\right)} = 97.370 \text{ mN/m}$$

The difference between the two scenarios is just 0.69%. It can be concluded that by assuming a circular cross section will introduce a very small amount of error compared to the elliptical cross section in this specific case were the variation of the radii is not too large.

4.3.2 Interface movement

Based on the method described in Section 3.3.4, the second analysis performed considers all the images taken in one period of the experiment. The behavior described in this Section is similar in all the fluids. For this reason it will be explained only one example with distilled water. Figure 37 shows four pictures where the movement of the interface can be seen. On each photography, two lines were established where the blue line is on the middle of the capillary tube and the red line is on the internal wall. After running the Matlab code that analyzes the gray intensity in each line, the plots on the bottom of the Figure 37 are obtained. The colors are in concordance for a better understanding: red for the inner wall and blue for the center.

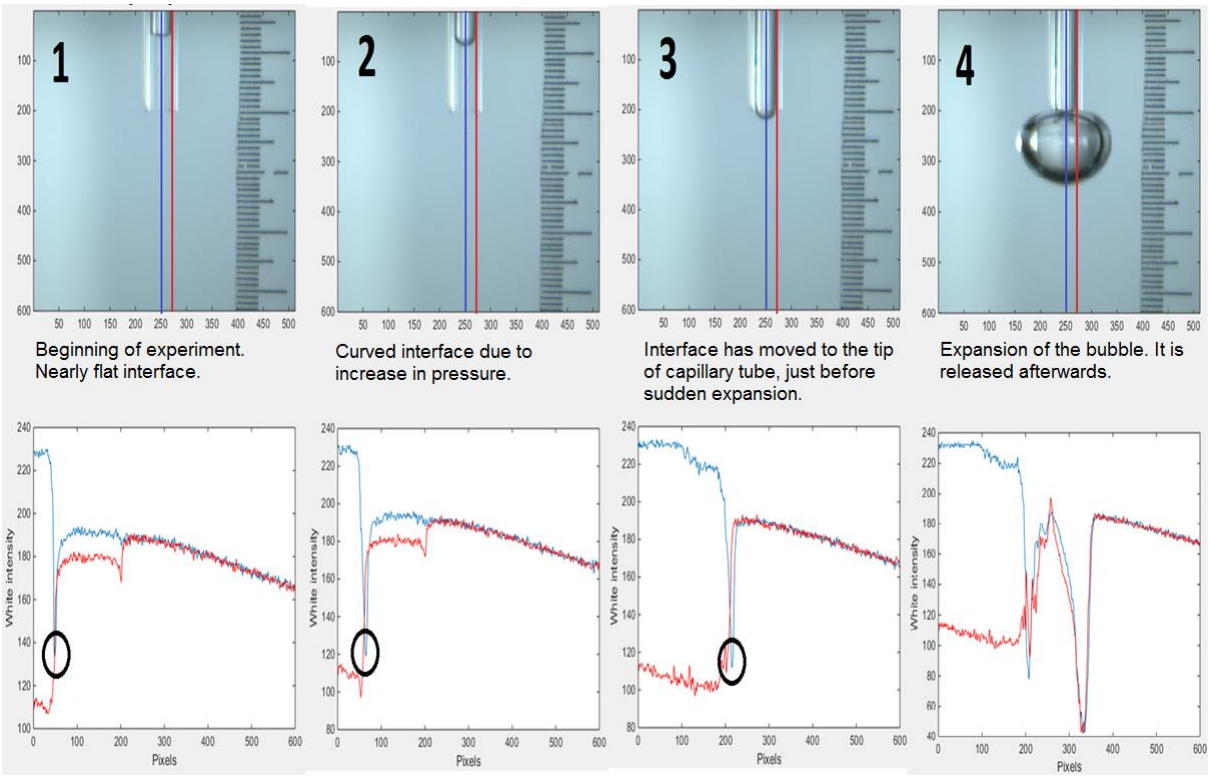

Figure 37: Movement of the interface along the time (top) with gray intensity analysis (bottom).

The image 1 shows the beginning of the experiment just at the moment the air pumping begins. The correspondant plot of the gray intensity is located below the same image. The interface shown by the image 1 is nearly flat. This is in concordance with the lower plot where the gray intensity on the blue line and the red line identify the interface at the same level. This part of the plot is highlighted with the black circle.

The image 2 shows an interface with a curvature due to the increase in the air pressure. The interface identified with the red line is above the interface identified with the blue line, as can be seen inside the black circle in the plot. This result is in concordance with the image.

After increasing the pressure, the curved interface moves to the tip of the capillary tube as shown in the image 3. This is the moment just before the bubble suddenly expands. Similar to the image 2, there is a difference in the location of the interface between the red line and the blue line that can be seen inside the black circle in the plot.

The bubble expands suddenly once the interface is released from the tip of the capillary tube, this can be seen on image 4. The lower plot shows two interfaces that correspond to the points where the blue and red lines cut the bubble on the image.

Since the analysis was performed on all the images in between the points mentioned in Figure 37, a plot that shows how the interface moves in a vertical axis along the time can be obtained. This plot is shown in Figure 38 left where the points 1, 2, 3 and 4 correspond to the ones mentioned on the Figure 37.

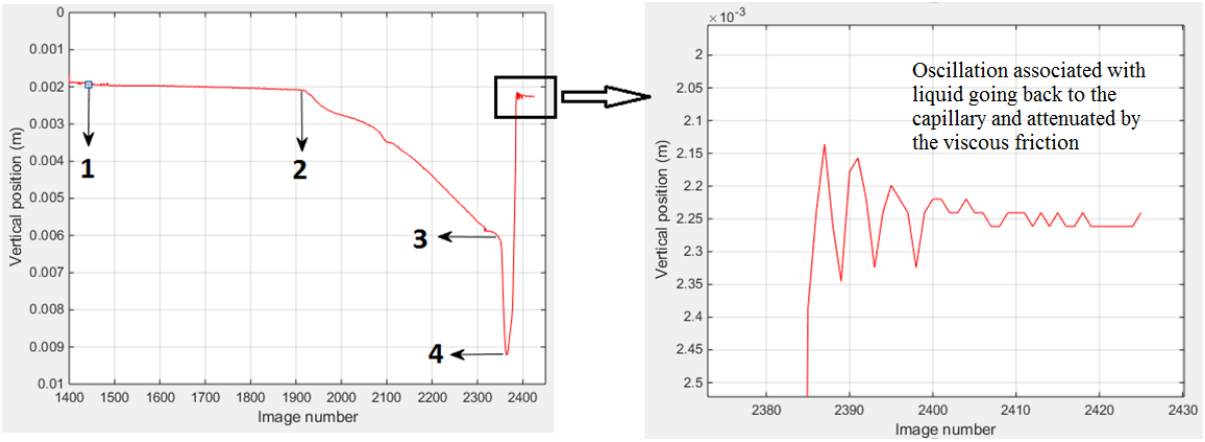

Figure 38: Position of the interface along the time.

From the point 1 to the point 2, it can be seen that the displacement of the interface is only 0.2 mm (from 1.9 mm to 2.1 mm) and it is mainly caused by the formation of the meniscus. From the point 2 to the point 3, the meniscus is displaced until the interface surpasses the tip of the capillary tube. The displacement is around 4 mm (from 2.1 mm to 6.1 mm). Between points 3 and 4, the bubble suddenly expands. The interface that now is located in the lowermost point of the bubble has moved 3.1 mm (from 6.1 mm to 9.2 mm). After this, the bubble leaves the capillary tube and moves to the surface.

A new cycle starts when the water rises again inside the tube. One peculiar singularity was observed when this happened. The equilibrium on the interface position is not reached instantaneously but oscillates. Figure 38 (right) shows the position of the interface along the time once the bubble is released, it can be seen that there is a harmonic oscillation. More specifically it is a lightly damped harmonic oscillator because it moves almost with the same frequency. But it loses amplitude and energy as the time goes on [24]. This is in concordance with the data presented on Figure 39. The oscillation can also be seen on the pressure data recorded with the absolute pressure sensor even after applying the filter (LPF).

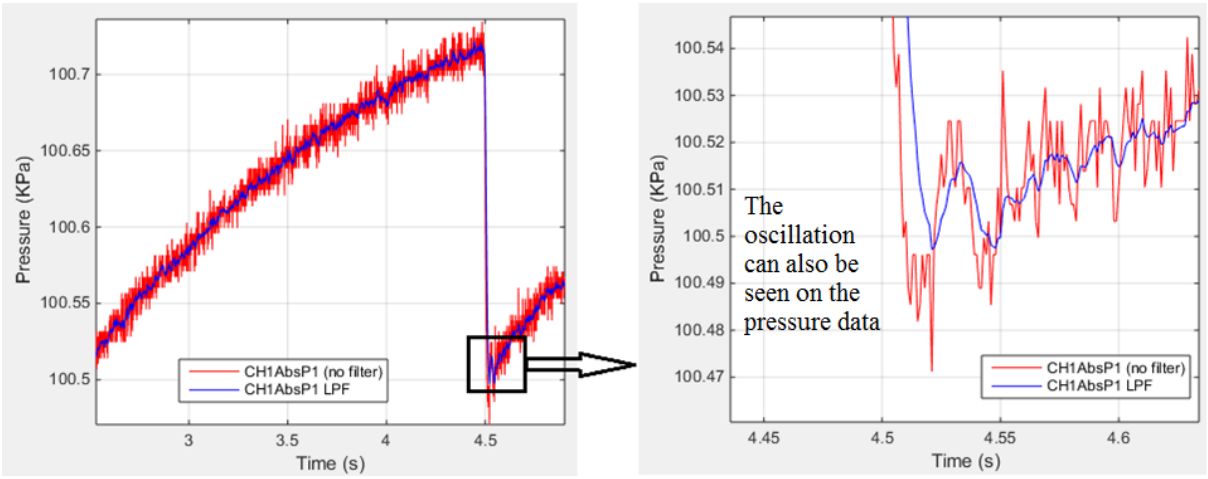

Figure 39: Absolute pressure 01 data showing oscillation.

4.4 Surface tension calculation

After performing the analysis of the quality of the data, it was decided to discard the absolute pressure 03 readings from the Absolute Pressure Temperature Sensor since the signal was noisy and the filters implemented didn't help on the signal improving. For this reason, the data recorded with the Dual Pressure Sensor was used to calculate the surface tension. More specifically the difference on the readings between the two pressure sensors because it was necessary to calculate the surface tension with the value of relative pressure to the atmosphere. Taking Figure 25 and Figure 28 as examples, it can be seen that there are around eight values of maximum pressure from Delta P. After applying the LPF and MAF, these values were averaged to obtain a single value of maximum pressure for each depth. These values were plotted against depth for each fluid and a linear regression was performed with the purpose of obtaining the equation of a straight line according to the procedure mentioned on the section 3.3.5. Finally, the surface tension σ and the correction factor β can be calculated for the different fluids.

4.4.1 Water

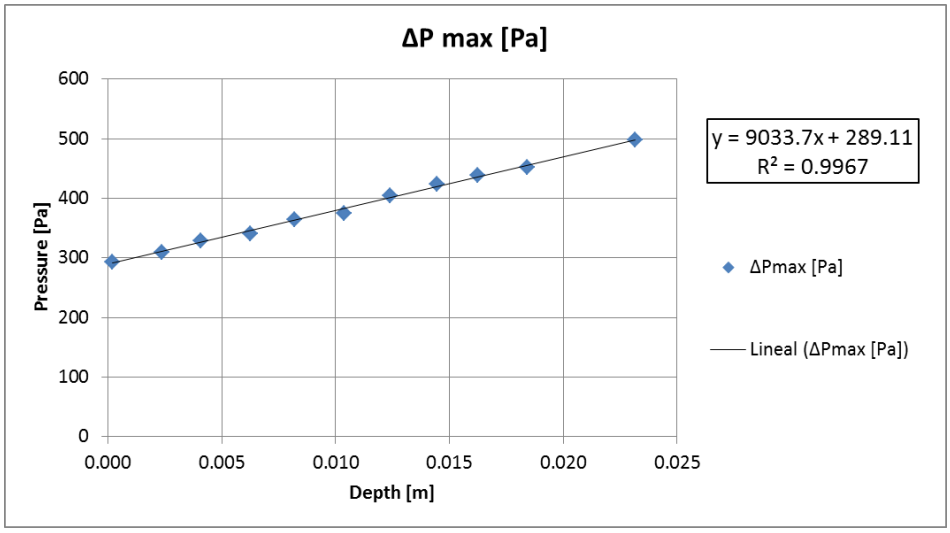

Figure 40: Max. Δ pressure vs. depth for water

The maximum values of pressure are plotted against depth in Figure 40. The equation obtained from the linear regression is $\Delta P_{max} = 9033.7\ h_A + 289.11$.

Comparing with the equation (7) $\Delta P_{MAX} = \frac{2 \cdot \sigma}{r} + \beta \cdot h_A \cdot \rho_A \cdot g$, the values are as follows:

$$\frac{2 \cdot \sigma}{r} = 289.11 \quad \text{and} \quad \beta \cdot \rho_A \cdot g = 9033.7$$

Considering a radius r = 0.489 mm, the surface tension calculated for water is σ = 70.68 mN/m at a temperature of 25.67 ˚C.

The density of water at the same temperature is 996.89 Kg/m^3 and the acceleration of gravity is 9.8 m/s^2. With these values, the correction factor for depth is calculated β = 0.9247.

The results are summarized in the Table 5.

Table 5: Surface tension calculation of water

Temperature T, ˚C	**Density @ T ρ_A, Kg/m^3**	**$\beta \cdot \rho_A \cdot g$**	**β**	**Radius *r*, mm**	**$\frac{2 \cdot \sigma}{r}$**	**Surface tension σ, mN/m**
25.67	996.89 [25]	9033.7	0.9247	0.489	289.11	70.68

Considering the theoretical values of surface tension from Table 2, it can be calculated at the temperature of 25.67 ˚C by an interpolation obtaining a value of 71.87 mN/m.

The difference between the theoretical and the experimental values of surface tension is 1.19 mN/m that represents an error of 1.66%.

4.4.2 Ethanol 30%w

Table 6: Surface tension calculation of ethanol 30%w

Temperature T, ˚C	Density @ T ρ_A, Kg/m^3	$\beta \cdot \rho_A \cdot g$	β	Radius *r*, mm	$\frac{2 \cdot \sigma}{r}$	Surface tension σ, mN/m
24.45	953.45 [26]	8218.2	0.8795	0.489	138.47	33.86

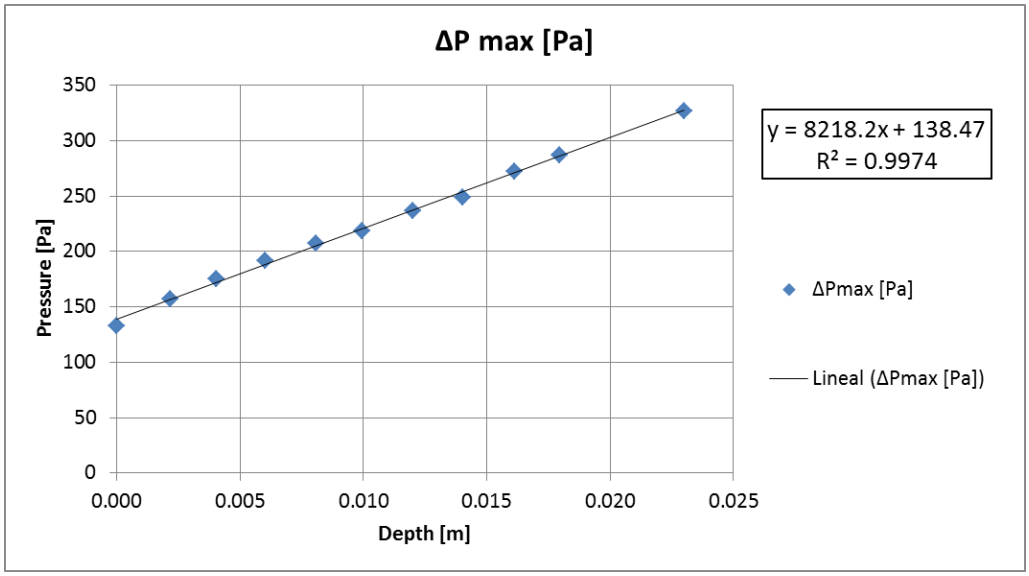

Figure 41: Max. Δ pressure vs. depth for ethanol 30%w

The equation obtained from the linear regression is $\Delta P_{max} = 8218.2\ h_A + 138.47$ from the data plotted in Figure 41.

Following the same procedure done with water, the calculations are performed and the results are shown on Table 6.

The theoretical value of surface tension is 33.04 mN/m at 24.45 ˚C, calculated by interpolation from the data shown on Table 2.

The difference between the theoretical and the experimental values of surface tension is 0.82 mN/m that represents an error of 2.48%.

4.4.3 Ethanol 10%w

Table 7: Surface tension calculation of ethanol 10%w

Temperature T, ˚C	Density @ T ρ_A, Kg/m^3	$\beta \cdot \rho_A \cdot g$	β	Radius *r*, mm	$\frac{2 \cdot \sigma}{r}$	Surface tension σ, mN/m
25.01	983.30 [26]	8713.3	0.9042	0.489	195.93	47.90

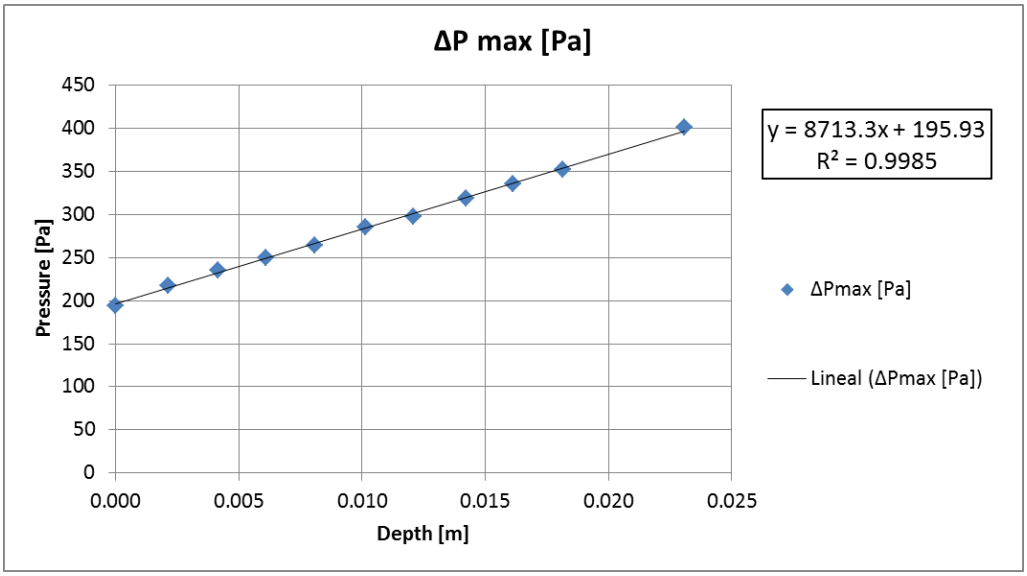

Figure 42: Max. Δ pressure vs. depth for ethanol 10%w

The equation obtained from the linear regression is $\Delta P_{max} = 8713.3\ h_A + 195.93$ from the data plotted in Figure 42.

Following the same procedure done with water, the calculations are performed and the results are shown on Table 7.

The theoretical value of surface tension is 48.21 mN/m at 25.01 ˚C, calculated by interpolation from the data shown on Table 2.

The difference between the theoretical and the experimental values of surface tension is 0.31 mN/m that represents an error of 0.64%.

4.4.4 n-Hexane

Table 8: Surface tension calculation of n-Hexane

Temperature T, ˚C	Density @ T ρ_A, Kg/m^3	$\beta \cdot \rho_A \cdot g$	β	Radius *r*, mm	$\frac{2 \cdot \sigma}{r}$	Surface tension σ, mN/m
25.69	655.80 [27]	5627.1	0.8756	0.489	70.746	17.29

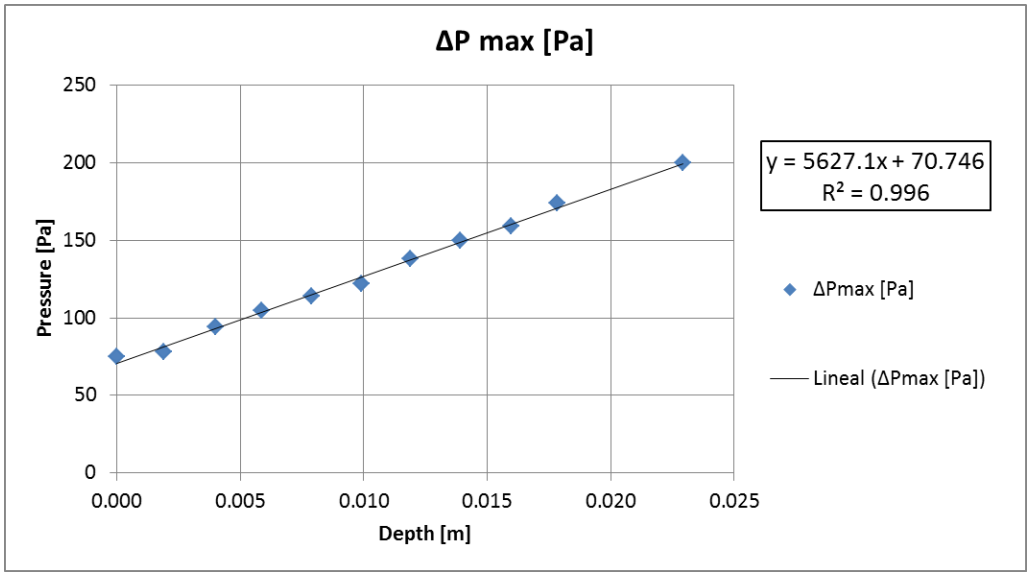

Figure 43: Max. Δ pressure vs. depth for n-Hexane

The equation obtained from the linear regression is $\Delta P_{max} = 5627.1\ h_A + 70.746$ from the data plotted in Figure 43.

Following the same procedure done with water, the calculations are performed and the results are shown on Table 8.

The theoretical value of surface tension is 17.81 mN/m at 25.69 ˚C, calculated by interpolation from the data shown on Table 2.

The difference between the theoretical and the experimental values of surface tension is 0.52 mN/m that represents an error of 2.92%.

4.4.5 n-Octane

Table 9: Surface tension calculation of n-Octane

Temperature T, ˚C	Density @ T ρ_A, Kg/m^3	$\beta \cdot \rho_A \cdot g$	β	Radius *r*, mm	$\frac{2 \cdot \sigma}{r}$	Surface tension σ, mN/m
26.10	698.60 [28]	6383.7	0.9324	0.489	80.698	19.73

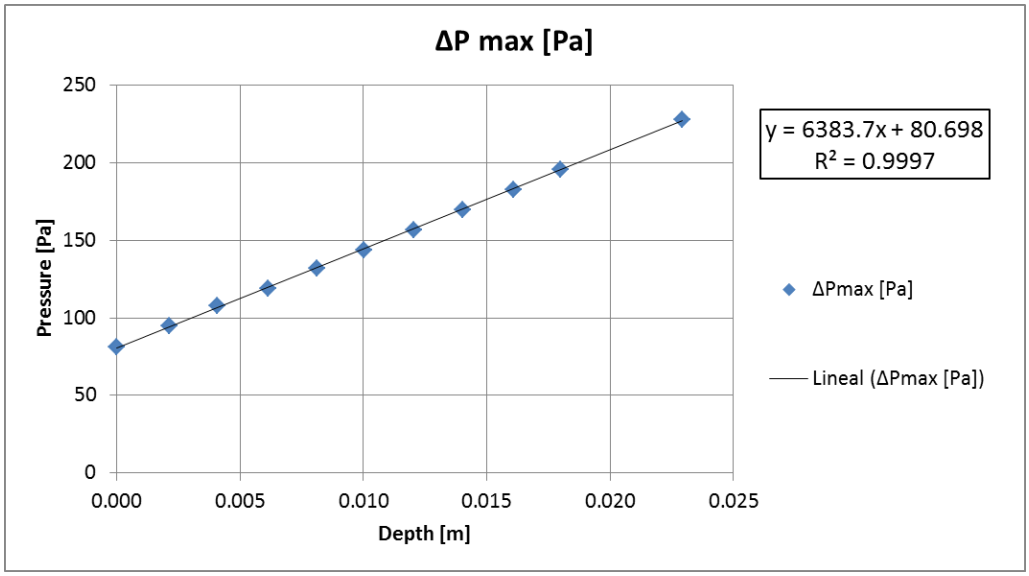

Figure 44: Max. Δ pressure vs. depth for n-Octane

The equation obtained from the linear regression is $\Delta P_{max} = 6383.7\ h_A + 80.698$ from the data plotted in Figure 44.

Following the same procedure done with water, the calculations are performed and the results are shown on Table 9.

The theoretical value of surface tension is 20.93 mN/m at 26.10 ˚C, calculated by interpolation from the data shown on Table 2.

The difference between the theoretical and the experimental values of surface tension is 1.2 mN/m that represents an error of 5.73%.

4.5 Summary of results and errors

Table 10: Summary of calculations and errors

Fluid	Temperature ˚C	Surface tension (theoretical) mN/m	Surface tension (experimental) mN/m	Correction factor β	% Error
Water	25.67	71.87	70.68	0.9247	1.66%
Ethanol 10%w	25.01	48.21	47.90	0.9042	0.64%
Ethanol 30%w	24.45	33.04	33.86	0.8795	2.48%
n-Octane	26.10	20.93	19.73	0.9324	5.73%
n-Hexane	25.69	17.81	17.29	0.8756	2.92%

Table 10 shows a summary of the main values obtained after performing the calculation of surface tension. It can be observed that the smallest error is 0.64% obtained from the experiment with Ethanol 10%w and the largest error is 5.73% obtained from the experiment performed with n-Octane. There are several variables that could cause this error. In the following lines, some possible reasons are explained.

The correction factor β doesn't have any relationship neither with the overall error nor the magnitude of the surface tension. This parameter is mainly introduced to adapt the equation from the theoretical values to the specific case of each experiment for each fluid at its given conditions.

The fluids were exposed to the atmosphere, since the quality of the air in the lab was not controlled, there is the possibility that some dust on the air fell inside the container, contaminating the surface of the fluid. Moreover, the nitrogen, the oxygen and other gases present on the air can react with the fluid and modify its surface tension.

The experiments were carried out exposed to a light source that according to the analysis it caused some temperature increase. Even though this increase was not large, it definitely introduced some error in the calculated values.

The measurement of the depth plays an important role on the method that was used in the experiments. The capillary tube is lowered inside the container until it touches the surface of the static fluid and this value is recorded as the initial depth. The fluid surface can have small waves induced by movement of air or vibrations from ground, this can lead to wrong values on depth measurement.

The initial reference level has a tendency to decrease since all of the fluids used on the experiment have some degree of volatility. Even though this was taken into account, some error linked to the measurement of the depth due to this phenomenon can affect the surface tension estimations.

From the image processing, it is observed that the radius of the capillary tube is not uniform and there are some fluctuations in this length. It was compared the calculations considering a circular shape and an elliptical shape, it was concluded that for small variations in radius the error introduced is less than 0.7% when considering a circular shape. Even though this value is not large, it definitely contributes on the overall error.

Once a bubble is released from the tip of the capillary tube, this travels to the surface and once it explodes, generates some waves on the surface of the fluid. This leads to fluctuations in the hydrostatic pressure and in the pressure recorded by the sensor.

There are some other possible reasons than can cause deviation from theoretical values such as the effect of gravity, bubble adhesion to capillary, particles of moisture carried by the air and turbulence generated by the growth of the bubble itself, among others [8].

Chapter 5

5. Conclusions

The surface tension was successfully measured by the use of the Maximum Bubble Pressure Method. The fast data recording for pressure, temperature and images played an important role in the achievement of the objectives. Five different fluids were used including distilled water and the results obtained doesn't show a large deviation from the theoretical values found on literature. All the efforts in order to have results as close as possible to the real ones were effective with errors no larger than 5.8%.

Large part of the time invested on this thesis was to build the setup. Many components were tested in order to meet the requirements for the experiment. The function of the air source worked as intended, the airflow could be controlled adequately. The plastic container was suitable to perform a good acquisition without blurry images of the bubbles. The connections between the air hoses showed some leakages at the beginning, this was fixed by changing the connection type, this could carry wrong pressure readings and at the end, wrong estimation in the value of surface tension.

The pressure and temperature recorded in the experiments was done by the use of sensors that had some associated noise when recording data. The use of filtering techniques and noise analysis proved to be a reliable method of treat the recordings in order to have data that reflect properly the reality. Even though the mathematical principles behind the noise analysis techniques are advanced, there are no fixed parameters or rules to be applied in order to affirm a good filtering of the signal. Good judgment and common sense played an important role and this can't be programed on a script.

It is strongly recommended to develop software to trigger at the same time the pressure and temperature recordings with the image acquisition. In this case it was not difficult to link the pictures with the pressure data since there are some points that can be easily identified that occur at the same time. This helps the correlation but in other applications probably this can't be done and it is crucial for a successful test.

It is important to be aware about all the variables that can affect the final results because any deviation from the theory of the MBPM can carry some errors. During the experiment, I tried to have the conditions as close as possible to what theory says. Despite this, there are some

deviations, these were analyzed and its impact to the calculations reduced in order to have accurate values. However, it is impossible to take into account all the variables that can affect the final results and the error introduced by this was just accepted. For further studies it is recommended to consider all the work done in this thesis in order to minimize the amount of error and increase the accuracy of the calculations.

By the use of Matlab in the image processing from slow-motion camera pictures demonstrates to be a useful tool to obtain length measurements along the time when the interface between air and liquid is moving inside the capillary tube. These images were linked to the pressure readings to perform a complete analysis of what is happening in the system. A particular phenomenon was observed when the bubble detaches from the tip of the capillary tube: the liquid rises rapidly inside the small tube and starts to oscillate because of the gas compressibility. By performing a specific analysis of this singularity some other fluid properties could be inferred. The scope of the present thesis does not consider this analysis but establish some basis for further work by studying this elastic effect.

References

1. Bush, P.J.W.M., MIT OCW: 18.357 Interfacial Phenomena, Lecture Notes. 2010.

2. Ross, J.L., W.D. Bruce, and W.S. Janna, Surface tension measurements of benzyl benzoate using the Sugden maximum bubble pressure method. Langmuir, 1992. 8(11): p. 2644-2648.

3. Time, R., Lecture notes from PET505 - Directional Drilling and Well Flow Engineering. 2016, Stavanger: University of Stavanger.

4. Adamson, A.W. and A.P. Gast, Physical chemistry of surfaces. Sixth ed. 1997, USA.

5. J Gloor, G., et al., An accurate density functional theory for the vapor-liquid interface of associating chain molecules based on the statistical associating fluid theory for potentials of variable range. Vol. 121. 2005. 12740-59.

6. Drelich, J., C. Fang, and C. White, Measurement of interfacial tension in Fluid-Fluid Systems. 2002. 3152-3166.

7. SITA, P.S. Bubble pressure method for measuring the dynamic surface tension. 2017; Available from: https://www.sita-process.com/information-service/process-parameter-surface-tension/bubble-pressure-method-for-measuring-the-surface-tension/.

8. Benedetto, F.E., H. Zolotucho, and M.O. Prado, Critical Assessment of the Surface Tension determined by the Maximum Pressure Bubble Method. Materials Research, 2015. 18: p. 9-14.

9. Sui, D., PET 525 Drilling Automation - Lecture Notes. 2017, Stavanger: University of Stavanger.

10. Nieto, A. Alguien ha hecho el vídeo perfecto para todos los que sufrimos intentando entender la Transformada de Fourier. 2018; Available from: https://m.xataka.com/otros/alguien-ha-hecho-el-video-perfecto-para-todos-los-que-sufrimos-intentando-entender-la-transformada-de-fourier.

11. Verpe, I. and M. Johnsen, Gas kick in vertical wells, an experimental study of gas kick. 2012.

12. Ovinger i bore - og bronnvaesker. 2012: Universitetet i Stavanger.

13. Johnsen, M.S., Particle Transport and Hole Cleaning in Wells During Drilling. 2014, University of Stavanger.

14. Petrova, T. and R.B. Dooley, Revised Release on Surface Tension of Ordinary Water Substance. International Association for the Properties of Water and Steam, 2014.

15. Vazquez, G., E. Alvarez, and J.M. Navaza, Surface Tension of Alcohol Water + Water from 20 to 50 degree C. Journal of Chemical Engineering, 1995: p. 611-614.

16. Queimadaa, A.J., I.M. Marrucho, and J.A.P. Coutinho, Surface tension of pure heavy n-alkanes: a corresponding states approach. 2001, Chemistry Department, University

of Aveiro, 3810-193 Aveiro, Portugal; and Centro de Investigação em Quimica, Chemistry Department, Faculty of Sciences, University ofPorto, 4169-007 Porto, Portugal.

17. Dortmund_Data_Bank. Surface Tension of Hexane. Available from: http://www.ddbst.com/en/EED/PCP/SFT_C89.php.

18. Cole-Parmer. Cole-Parmer Compact Bottletop Dispenser Specs. 2018; Available from: https://www.coleparmer.com/i/cole-parmer-compact-bottletop-dispenser-2-to-10-ml/0791640.

19. HTC_Corporation. HTC 10 specs. 2018; Available from: https://www.htc.com/us/smartphones/htc-10/.

20. Basler. acA800-510uc - Basler ace specs. 2018; Available from: https://www.baslerweb.com/en/products/cameras/area-scan-cameras/ace/aca800-510uc/.

21. US Department of Energy, Lighting Choices to Save You Money. 2018. Cited 2018; Available from: https://www.energy.gov/energysaver/save-electricity-and-fuel/lighting-choices-save-you-money.

22. LABINO_AB. LABINO compact lamps data sheet. Available from: http://www.grimas.hu/wp-content/uploads/2014/03/Labino_UV_reflektor_135-230V.pdf.

23. PASCO. 850 Universal Interface - UI-5000 Specs. 2018; Available from: https://www.pasco.com/prodCatalog/UI/UI-5000_850-universal-interface/index.cfm.

24. Richmond, M. Theory of Damped Harmonic Motion. Available from: http://spiff.rit.edu/classes/phys312/workshops/w5b/damped_theory.html.

25. Walker, R. Density, sg of water at different temps. 2015. Cited 2018; Available from: https://www.simetric.co.uk/si_water.htm.

26. Speight, J.G., Lange's handbook of chemistry. Vol. 1. 2005: McGraw-Hill New York.

27. Bank, D.D. Density of Hexane. Cited 2018; Available from: http://www.ddbst.com/en/EED/PCP/DEN_C89.php.

28. Information, N.C.f.B. PubChem Compound Database; CID=356. Octane. Cited 2018; Available from: https://pubchem.ncbi.nlm.nih.gov/compound/octane.

Appendices

Appendix A: Matlab Scripts

A1. Importing data

```
clear, clc, close all
%% Import data from text file.
% Auto-generated by MATLAB on 2018/06/12 23:31:14

%% Initialize variables.
filename = 'Experiment 06.txt';
delimiter = '\t';
startRow = 3;

%% Read columns of data as strings:
% For more information, see the TEXTSCAN documentation.
formatSpec = '%s%s%s%s%s%s%[^\n\r]';

%% Open the text file.
fileID = fopen(filename,'r');

%% Read columns of data according to format string.
% This call is based on the structure of the file used to generate this
% code. If an error occurs for a different file, try regenerating the code
% from the Import Tool.
dataArray = textscan(fileID, formatSpec, 'Delimiter', delimiter,
'HeaderLines' ,startRow-1, 'ReturnOnError', false);

%% Close the text file.
fclose(fileID);

%% Convert the contents of columns containing numeric strings to numbers.
% Replace non-numeric strings with NaN.
raw = repmat({''},length(dataArray{1}),length(dataArray)-1);
for col=1:length(dataArray)-1
    raw(1:length(dataArray{col}),col) = dataArray{col};
end
numericData = NaN(size(dataArray{1},1),size(dataArray,2));

for col=[1,2,3,4,5,6]
    % Converts strings in the input cell array to numbers. Replaced non-
numeric
    % strings with NaN.
    rawData = dataArray{col};
    for row=1:size(rawData, 1);
        % Create a regular expression to detect and remove non-numeric
prefixes and
        % suffixes.
        regexstr = '(?<prefix>.*?)(?<numbers>([-
]*(\d+[\,]*)+[\.]{0,1}\d*[eEdD]{0,1}[-+]*\d*[i]{0,1})|([-
]*(\d+[\,]*)*[\.]{1,1}\d+[eEdD]{0,1}[-+]*\d*[i]{0,1}))(?<suffix>.*)';
        try
            result = regexp(rawData{row}, regexstr, 'names');
            numbers = result.numbers;

            % Detected commas in non-thousand locations.
```

```
            invalidThousandsSeparator = false;
            if any(numbers==',');
                thousandsRegExp = '^\d+?(\,\d{3})*\.{0,1}\d*$';
                if isempty(regexp(thousandsRegExp, ',', 'once'));
                    numbers = NaN;
                    invalidThousandsSeparator = true;
                end
            end
            % Convert numeric strings to numbers.
            if ~invalidThousandsSeparator;
                numbers = textscan(strrep(numbers, ',', ''), '%f');
                numericData(row, col) = numbers{1};
                raw{row, col} = numbers{1};
            end
        catch me
        end
    end
end

%% Replace non-numeric cells with NaN
R = cellfun(@(x) ~isnumeric(x) && ~islogical(x),raw); % Find non-numeric
cells
raw(R) = {NaN}; % Replace non-numeric cells

%% Allocate imported array to column variable names
Time = cell2mat(raw(:, 1));
CH1AbsP1 = cell2mat(raw(:, 2));
CH1AbsP2 = cell2mat(raw(:, 3));
CH2AbsP_raw = cell2mat(raw(:, 4));
CH2Temp_raw = cell2mat(raw(:, 5));
CH1DeltaP = cell2mat(raw(:, 6));


%% To extract the values with a 100 Hz frequency
n=floor(length(Time)/10);
for i=1:n
    CH2AbsP(i)=CH2AbsP_raw(1+10*i);
    CH2Temp(i)=CH2Temp_raw(1+10*i);
    Time_100Hz(i)=Time(1+10*i);
end
%% Clear temporary variables
clearvars CH2AbsP_raw CH2Temp_raw i n filename delimiter startRow
formatSpec fileID dataArray ans raw col numericData rawData row regexstr
result numbers invalidThousandsSeparator thousandsRegExp me R;
```

A2. Fast Fourier Transform

```
%% FFT analysis of the signal during the experiment
close all, clc
Fs = 1000;                    % Sampling frequency, 1 KHz in this case
T = 1/Fs;                     % Sample time
L = length(CH1AbsP1);         % Length of signal
t = (0:L-1)*T;                % Time vector
% To normalize the data
ynew1=CH1AbsP1-mean(CH1AbsP1);
ynew2=CH1AbsP2-mean(CH1AbsP2);
ynew3=CH1DeltaP-mean(CH1DeltaP);

%% Appliying the FFT
NFFT = 2^nextpow2(L); % Next power of 2 from length of y, it is the same
for all the readings
Y1 = fft(ynew1,NFFT)/L;
f1 = Fs/2*linspace(0,1,NFFT/2+1);
Y2 = fft(ynew2,NFFT)/L;
f2 = Fs/2*linspace(0,1,NFFT/2+1);
Y3 = fft(ynew3,NFFT)/L;
f3 = Fs/2*linspace(0,1,NFFT/2+1);

%% Ploting the results.
figure (1)
subplot(3,1,1)
plot(f1,2*abs(Y1(1:NFFT/2+1)))
title('CH1AbsP1 - Single-Sided Amplitude Spectrum of y(t)')
xlabel('Frequency (Hz)')
ylabel('Amplitude')
grid on

subplot(3,1,2)
plot(f2,2*abs(Y2(1:NFFT/2+1)))
title('CH1AbsP2 - Single-Sided Amplitude Spectrum of y(t)')
xlabel('Frequency (Hz)')
ylabel('Amplitude')
grid on

subplot(3,1,3)
plot(f3,2*abs(Y3(1:NFFT/2+1)))
title('CH1DeltaP - Single-Sided Amplitude Spectrum of y(t)')
xlabel('Frequency (Hz)')
ylabel('Amplitude')
grid on


clearvars f1 f2 f3 Fs L NFFT t T Y1 Y2 Y3 ynew1 ynew2 ynew3
```

A3. Low Pass Filter

Low Pass Filter function

```
function y =lowpassFilter(x,dt,timeConstant)
%x calls hte input vector
%dt time interval, commonly 1
alpha = dt / (timeConstant + dt);
y(1) = x(1);
n=length(x);
for i=2:n
    y(i) = alpha * x(i) + (1-alpha) * y(i-1);
end
end
```

Low Pass Filter script

```
%% Low pass filter
close all, clc
w=10; %defines the cutout frequency
CH1AbsP1_LPF = lowpassFilter(CH1AbsP1,1,w);
CH1AbsP2_LPF = lowpassFilter(CH1AbsP2,1,w);
CH1DeltaP_LPF = lowpassFilter(CH1DeltaP,1,w);
CH2AbsP_LPF = lowpassFilter(CH2AbsP,1,w);
CH2Temp_LPF = lowpassFilter(CH2Temp,1,w);
clearvars w

figure(1)
subplot(2,2,1)
plot (Time,CH1AbsP1,'r',Time,CH1AbsP1_LPF,'b');
xlabel('Time (s)');
ylabel('Pressure (KPa)');
grid on;
legend('CH1AbsP1 (no filter)','CH1AbsP1 LPF');
title('Dual pressure sensor - P.Abs 01')

subplot(2,2,2)
plot (Time,CH1AbsP2,'r',Time,CH1AbsP2_LPF,'b');
xlabel('Time (s)');
ylabel('Pressure (KPa)');
grid on;
legend('CH1AbsP2 (no filter)','CH1AbsP2 LPF');
title('Dual pressure sensor - P.Abs 02')

subplot(2,2,3)
plot (Time,CH1DeltaP,'r',Time,CH1DeltaP_LPF,'b');
xlabel('Time (s)');
ylabel('Pressure (KPa)');
grid on;
legend('CH1DeltaP (no filter)','CH1DeltaP LPF');
title('Dual pressure sensor - Delta P')

subplot(2,2,4)
plot (Time_100Hz,CH2AbsP,'r',Time_100Hz,CH2AbsP_LPF,'b');
xlabel('Time (s)');
ylabel('Pressure (KPa)');
grid on;
legend('CH2AbsP (no filter)','CH2AbsP LPF');
title('Abs. pressure temperature sensor - P. Abs')

figure(2)
plot(Time_100Hz,CH2Temp,'r')
```

```
hold;
plot(Time_100Hz,CH2Temp_LPF,'b')
title('Temperature')
xlabel('Time')
ylabel('deg C')
%axis([0 10 25.91 25.94])
grid on
```

A4. Moving Average Filter

```
%% Moving average filter
close all, clc
N=50; %consecutive samples to be averaged
coef=ones(1,N)/N;
CH1AbsP1_MAF=filter(coef,1,CH1AbsP1);
CH1AbsP2_MAF=filter(coef,1,CH1AbsP2);
CH1DeltaP_MAF=filter(coef,1,CH1DeltaP);
CH2AbsP_MAF=filter(coef,1,CH2AbsP);
CH2Temp_MAF=filter(coef,1,CH2Temp);
 clearvars N coef
%% For plotiing
figure(1)
subplot(2,2,1)
plot(Time,CH1AbsP1,'r')
hold;
plot(Time,CH1AbsP1_MAF,'b')
axis([0 10 101.56 101.68])
xlabel('Time (s)')
ylabel('Pressure (KPa)')
legend('CH1AbsP1 (no filter)','CH1AbsP1 MAF')
grid on
title('Dual pressure sensor - P.Abs 01')

subplot(2,2,2)
plot(Time,CH1AbsP2,'r')
hold;
plot(Time,CH1AbsP2_MAF,'b')
axis([0 10 101.45 101.55])
xlabel('Time (s)')
ylabel('Pressure (KPa)')
legend('CH1AbsP2 (no filter)','CH1AbsP2 MAF')
grid on
title('Dual pressure sensor - P.Abs 02')

subplot(2,2,3)
plot(Time,CH1DeltaP,'r')
hold;
plot(Time,CH1DeltaP_MAF,'b')
axis([0 10 0.05 0.2])
xlabel('Time (s)')
ylabel('Pressure (KPa)')
legend('CH1DeltaP (no filter)','CH1DeltaP MAF')
grid on
title('Dual pressure sensor - Delta P')

subplot(2,2,4)
plot(Time_100Hz,CH2AbsP,'r')
hold;
plot(Time_100Hz,CH2AbsP_MAF,'b')
axis([0 10 101.72 101.86])
xlabel('Time (s)')
ylabel('Pressure (KPa)')
legend('CH2AbsP (no filter)','CH2AbsP MAF')
grid on
title('Abs. pressure temperature sensor - P. Abs')

figure(2)
plot(Time_100Hz,CH2Temp,'r')
```

```
hold;
plot(Time_100Hz,CH2Temp_MAF,'b')
title('Temperature')
xlabel('Time')
ylabel('deg C')
legend('CH1Temp (no filter)','CH1DeltaP MAF')
axis([0 10 26.1 26.14])
grid on
```

A5. Image Processing

```
%% Image analysis for Surface tension analysis
clear all, clf, clc, close all
file_name = ('Basler acA800-510uc (21763331)_20180314_181509463_0001.tiff')
%  Read image "filename" with format = height x width x color: <352x1024x3
uint8>
Bilde=imread(file_name);
%% ************* Original image  ****************************
figure(1)
image(Bilde)
title('Original image in color')
%% ************* Original image converted to gray ********************
figure(2)
% "Graybilde" er bedre å bruke enn de splittede ss variantene for å se
% detaljer.
Graybilde = rgb2gray(Bilde);
subplot(2,1,1)
hold off
imshow(Graybilde) %Seems to be necessary to enable the hi-res gray scale
image(Graybilde)
hold on
title('Image with pathlines along meter stick')
nl=3;
konv1 = 12.25e-3/586;   %conversion between length and pixels
konvert=konv1;
Lengde0 = 1:600; %vertical resoluction of image
Lengde=Lengde0*konvert;
Linje = [410 450 485]; %indicates the pixel column where you want to
perform the readings
Len =[0.1 0.2 0.4];
for ie = 1:3
Skalfarge(ie,:)=Graybilde(:,Linje(ie));
end
for jl=1:3
    for il=1:600
    Merkemm(jl,il)=0;
    if Skalfarge(jl,il)<122; %122 is limit of gray intensity
        Merkemm(jl,il)=0.1;
    end
    end
end
subplot(2,1,2)
% Plot scaler marks
plot(Lengde,Merkemm(1,:),'-r')
hold on
plot(Lengde,Len(2)+ Merkemm(2,:),'-b')
plot(Lengde,Len(3)+ Merkemm(3,:),'-k')
axis([0 1.3e-2 0 0.6])
xlabel('meters')
grid on
subplot(2,1,1)  %position and amplitude of where to show the line
plot(Merkemm(1,:)*150+410,Lengde0,'-r')
plot(Merkemm(2,:)*150+450,Lengde0,'-b')
plot(Merkemm(3,:)*150+485,Lengde0,'-k')
xlabel('pixels')
ylabel('pixels')
hold off

%% Read sequence to detect interface
```

```
for i=2550:3420; %one cycle of images
        foth=floor(i/1000)*1000; thrd=floor(i/100)*100;
secnd=floor(i/10)*10; fist=i;
        k=fist-secnd; j=(secnd-thrd)/10;l=(thrd-foth)/100;m=foth/1000;
file_name = sprintf('Basler acA800-510uc
(21763331)_20180314_181509463_%d%d%d%d.tiff',m,l,j,k);
% "Basler acA800-510uc (21763331)_20180314_181509463_2550.tiff" is the
% initial image
% "Basler acA800-510uc (21763331)_20180314_181509463_3420.tiff" is the last
% image
%  Read image "filename" with format = height x width x color: <352x1024x3
uint8>
Bilde=imread(file_name);
figure(3) %initial image
image(Bilde)
title('new  - Original image in color')
drawnow
figure(4) %movement of the interface while processing
subplot(3,1,1)
image(Bilde)
title('Original image in color')
subplot(3,1,2)
Graybilde2 = rgb2gray(Bilde);
Interfarge =Graybilde2(:,249); %position of interface line at center
Veggfarge = Graybilde2(:,267); %position of interface line at sidewall
plot(Interfarge)
hold on
plot(Veggfarge,'-r')
ylabel('White intensity')
xlabel('Pixels')
hold off
    for il=1:600
    Interface(il)=0;
    if Interfarge(il)<130 %intensity of gray
        Interface(il)=1;
    end
    end
[Gram,Gimin(i)]=min(Interfarge);
kant(i) = find(Veggfarge < 130,1,'last');  % Detect the interface at
sidewall
subplot(3,1,3)
plot(Interface)
hold on
end
figure(5) ; %Vertical position of intherphase in pixels
plot(Gimin,'.')
plot(kant,'-r')
hold on
hold off
ylabel('Vertical position (pix)')
xlabel('Image number')
figure(6) % Vertical position of intherphase in meters
plot(konvert*Gimin,'.')
plot(konvert*kant,'-r')
hold on
axis([2500 3500 0 0.008 ])
hold off
ylabel('Vertical position [m]')
xlabel('Image number')
figure(7) %  Show the principal images from experiment
for i=2450:3420
```

```
            foth=floor(i/1000)*1000; thrd=floor(i/100)*100;
secnd=floor(i/10)*10; fist=i;
        k=fist-secnd; j=(secnd-thrd)/10;l=(thrd-foth)/100;m=foth/1000;
file_name = sprintf('Basler acA800-510uc
(21763331)_20180314_181509463_%d%d%d%d.tiff',m,l,j,k);
%  Read image "filename" with format = height x width x color: <352x1024x3
uint8>
Bilde=imread(file_name);
if i==2450
    subplot(2,2,1)
    image(Bilde)
    title(['Image : ' num2str(i) ])
elseif i==3046
    subplot(2,2,2)
    image(Bilde)
    title(['Image : ' num2str(i)  ])
elseif i==3357
    subplot(2,2,3)
    image(Bilde)
    title(['Image : ' num2str(i)  ])
elseif i==3370
    subplot(2,2,4)
    image(Bilde)
    title(['Image : ' num2str(i)  ])
else
end
if i==3370
    Svarthvitt= im2bw(Bilde);
    figure(8)
    imshow(Svarthvitt)
end
end
```

Appendix B: Illustrations

Figure 45: Camera recording images from the tip of capillary tube

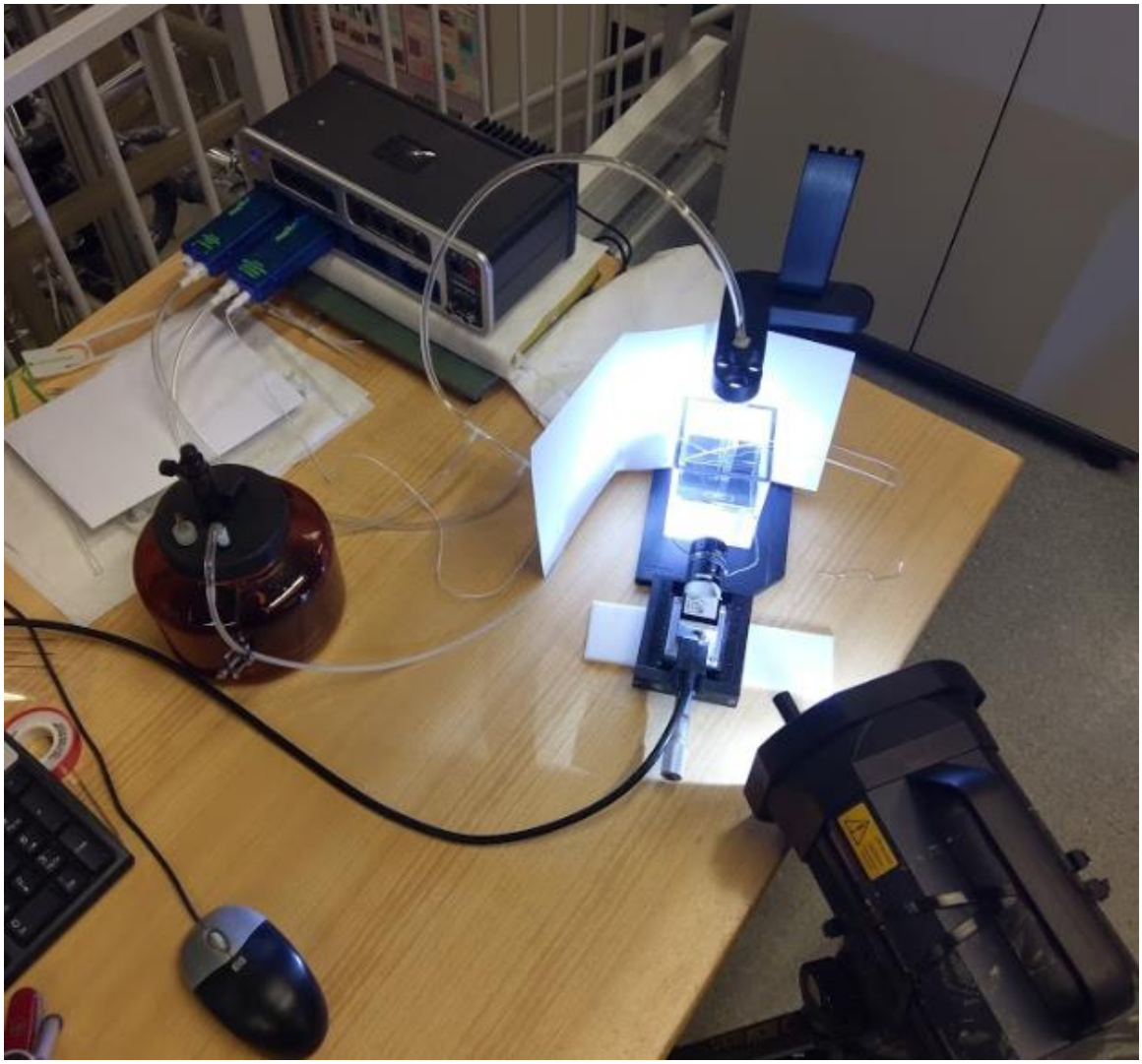

Figure 46: Final layout with all the equipment assembled